UNIVERSIDAD NACIONAL AUTÓNOMA DE MÉXICO

PROGRAMA DE MAESTRÍA Y DOCTORADO EN INGENIERÍA

INGENIERÍA ELÉCTRICA – SISTEMAS ELÉCTRICOS DE POTENCIA

FINITE ELEMENT ANALYSIS OF DISTRIBUTION TRANSFORMER UNDER HARMONICS CONDITION

TESIS
QUE PARA OPTAR POR EL GRADO DE:
DOCTOR EN INGENIERÍA

PRESENTA:
M. EN I. SOHAIL KHAN

TUTOR PRINCIPAL
DR. RAFAEL ESCARELA PÉREZ, UAM-AZCAPOTZALCO
COMITÉ TUTOR
DR. JUAN CARLOS OLIVARES GALVÁN, UAM-AZCAPOTZALCO
DR. FRÉDÉRIC TRILLAUD, INSTITUTO DE INGENIERÍA UNAM
DR. PAUL ROLANDO MAYA ORTIZ, INSTITUTO DE INGENIERÍA UNAM

CIUDAD DE MÉXICO, NOVIEMBRE 2021

JURADO ASIGNADO:

Presidente:	Dr. Paul Rolando Maya Ortiz
Secretario:	Dr. Frederic Trillaud
1er. Vocal:	Dr. Rafael Escarela Pérez
2do. Vocal:	Dr. Juan Ramón Rodriguez Rodriguez
3er. Vocal:	Dr. Juan Carlos Olivares Galván

Lugar o lugares donde se realizó la tesis: Ciudad de México

TUTOR DE TESIS:

NOMBRE

Dr. Rafael Escarela Pérez
FIRMA

DEDICATION

I dedicate this thesis to my Professors, friends and family members.

Acknowledgement

First of all, I am thankful to my supervisor Dr. Rafael Escarela Perez for his tremendous support towards realizing my dream to get a Doctorate degree in Electrical Engineering. His supervision and suggestions always enriched my knowledge and skills.

I would like to extend my special thanks to PhD committee, that include Dr. Juan Carlos Olivares Galvan, Frederic Trillaud, and Paul Rolando Maya Ortiz who always came up with interesting questions in the exams. Their questions and suggestions always gave me the right direction towards carrying out a research work and writing my thesis. I am also thankful to Professor Juan Ramon Rodriguez who revised my thesis and suggested me changes to improve the quality of my thesis.

The supersvision of Dr. Serguei Maximov indeed helped to obtain Mathematical formulation and include it in this thesis. I am also thankful to Dr. David Granados Lieberman who supported me in the experimental work.

Special thanks to the National Council of Science and Technology (CONACYT), for the support awarded through the scholarship for postgraduate studies, from September 2017 to August 2021 (CVU 828886).

Last but not the least, I am thankful to my dear Maria de Lourdes Rivera Perez for her patience and unlimited support. Thanks also to my Mother, Father, Brothers, and my only sister whose hearts are always with me and whose prayers light my way in this life.

Resumen

El uso generalizado de cargas y sistemas no lineales en la red eléctrica ha dado lugar a problemas de calidad de la energía. Uno de los problemas de calidad de la energía es la generación de armónicos en corrientes y voltajes. Estas corrientes y voltajes generan pérdidas adicionales en los transformadores. En esta tesis se realiza un estudio exhaustivo del problema armónico en transformadores. Se han revisado los modelos matemáticos ampliamente utilizados en la literatura para evaluar los efectos armónicos. Adicionalmente, se han establecido las acciones probadas consideradas en la industria para reducir estos efectos, que ayudarán a los diseñadores de la industria. Entre las estrategias implementadas en la industria, se ha presentado una revisión del estado del arte de la reducción y dimensionamiento de transformadores. Al realizar dicho estudio se presenta un panorama general del problema y sus soluciones.

Las regiones de boquillas del transformador, que incluyen boquillas y paredes de tanques, son quizás una de las partes más expuestas a la inducción electromagnética de los conductores que pasan a través de las boquillas de los transformadores de potencia, y en los regímenes de armónicos, estas partes son más propensas a sobrecalentarse. Por lo tanto, se realiza un análisis en profundidad de las pérdidas de la pared del tanque del transformador debido a los armónicos utilizando un enfoque analítico. Se logra resolviendo las ecuaciones de Maxwell con sus correspondientes condiciones de frontera. La ecuación diferencial así obtenida se resuelve mediante el método de separación de variables. Las fórmulas obtenidas se evalúan para diferentes contenidos de armónicos de la corriente de carga y pérdidas. Los resultados concuerdan con las simulaciones realizadas con software de elementos finitos (FE).

Además, se establece una configuración experimental que posibilita la generación de armónicos. Las formas de onda de voltaje distorsionadas se generan experimentalmente y se pasan a través del transformador y las pérdidas se calculan utilizando la Transformada de Fourier de Corto Tiempo. La estrategia se ejemplifica en un transformador de tipo seco de 200 VA que suministra energía a una carga resistiva.

Abstract

The widespread use of non-linear loads and systems in power network has resulted in power quality problems. The distortion in currents and voltages is one of them, which results in power losses, increasing temperature, and accelerated loss of life (LOL) in transformers. In this document, the impacts of harmonics and interharmonics on transformers are reviewed. To lessen these impacts and avoid premature transformer damage, possible modifications in transformer design practices are discussed. This would help industrial transformer designers to face new power system demands. A state-of-the-art review of techniques, such as resizing and derating, is presented.

Bushing regions of transformer, that include bushings and tank walls, are perhaps one of the weakest parts of power transformers, and in harmonics regimes, these parts are more prone to fail. Therefore, an in-depth analysis of transformer tank wall losses due to harmonics is done using analytical approach. It is achieved by solving Maxwell's equations with their corresponding boundary conditions. The differential equation thus obtained is solved using the method of separation of variables. The obtained formulas are evaluated for different harmonics of the load current and losses. The results are in good agreement with simulations carried out using finite element (FE) software.

Moreover, an experimental setup is established that makes possible the generation of harmonics. The distorted voltage waveforms are generated experimentally and are passed through the transformer and the losses are computed using Short Time Fourier Transform. The strategy is exemplified on a 200 VA dry-type transformer supplying power to a resistive load.

TABLE OF CONTENTS

LIST OF FIGURES

LIST OF TABLES

NOMENCLATURE

The symbols that denote a vector quantity are written in bold (**A**), while the Scalar quantities appear in italics or italics (*A*).

Symbol	Unit	Description
THD		Total harmonic distortion
$TIHD$		Total interharmonic distortion
THD_{total}		Total harmonic and interharmonic distortion
h		Harmonic order
k		Interharmonic
P_{EC}	Watt	Winding eddy current losses
P_{EC-O}	Watt	Winding eddy current losses at a fundamental frequency
I	Ampere	Current
F_{HL}		Harmonic loss factor
F_{HL-STR}		Harmonic loss factor for stray losses
δ	m	Depth of penetration
P	Watt	Power losses
R_{dc}	Ohms	dc resistance
Ke and K_h		Material dependent constants
f	Hz	Frequency
t	m	Thickness of lamination strips
n		Steinmetz constant
b	m	Width
d	m	Thickness
ρ	$\mathrm{Ohm-meter}$	Resistivity
H_0		Statistical distribution of the internal domain walls field
n		Harmonics
D	$\mathrm{C}/\mathrm{m^2}$	Electric field density
B	T	Magnetic field density
E	V/m	Electric Field
H	A/m	Magnetic field intensity
∇		Nabla operator
j	$\mathrm{A}/\mathrm{m^2}$	Current density
A	wb/m	Magnetic vector potential
ε	F/m	Electric permittivity
μ	H/m	Permeability
μ_0	H/m	Absolute permeability
μ_r		Relative permeability

σ	$S/_{m}$	Conductivity
$I_1(\lambda_{n,m}r)$ and $K_1(\lambda_{n,m}r)$		Modified Bessel functions of the first order
j		Imaginary number
ω	$rad/_{second}$	Angular frequency
HVDC		High Voltage Direct Current
EMF		Electromagnetic Field
EC		Eddy Currents
WEC		Winding Eddy Current
TSFEM		Time Stepping Finite Element Method

Chapter 1. INTRODUCTION

The growing energy demand and environmental problems have led to the integration of renewable energy technologies to the power grid. These technologies are integrated into the power system via inverters, requiring HVDC system for long-distance transmission. Their development over the past few decades, together with the non-linear loads such as inverters, arc furnaces, personal computers, AC and DC drives, etc. have brought about a significant increase in harmonics. Nonlinear loads are notorious for generating harmonics and require transformers to connect them safely to the power network.

Transformers are one of the most important and expensive assets of the power system that bridge generation and load [1]. Their reliable operation and efficiency are imperative for both electric power industries and users. They are usually designed under the assumptions of nominal voltage, rated frequency, balanced condition, and pure sinusoidal voltages and currents [2],[3]. The widespread use of non-linear loads and increase of renewable energy integration into power systems has led to distortion in voltage and current, causing power quality problems [4]. These effects cause significant impacts on transformers, resulting in accelerated loss of life (LOL) and, eventually, premature damage.

Harmonics are components appearing in the power system at frequencies that are multiple of the fundamental one. Their sources are converters, arc furnaces, static VAR compensators, distributed generation systems, controllers, cycloconverters, rectifiers, and Pulse Width Modulation (PWM) motor drives [5],[6]. Harmonics from the 3rd to the 25th, are the most common frequencies, prevailing in the distribution system [6]. The harmonic and interharmonic limits for different voltage levels in power systems are established in the IEEE standard [5].

1.1 MOTIVATION

Transformers are usually designed under the assumptions of sinusoidal conditions [7], [8]. With the increasing trend of non-linear loads in power system, the transformer design process must include the distortion in the current and voltage to ensure the transformer efficiency and reliability. It is known that the harmonic content in the load current increases losses and temperature in the transformers, resulting in their premature damage [7].

Bushings are perhaps the weakest parts of transformers, electrically and physically, and their failure is one of the major causes of transformer malfunctions. The contribution of bushings and tank walls to transformer failures are about 20 % and 21%, respectively, which is a significant percentage among all the damages caused by other parts of transformer [9]. Therefore, with the increasing trend of non-linear loads in the distribution network, the transformer is even more prone to failure. Hence, it is very important to study the harmonics effect in different parts of transformer.

1.2 STATE OF THE ART

Transformers subjected to harmonic currents and voltages suffer thermal stresses due to the additional losses. Therefore, it is necessary to present a comprehensive literature survey of the harmonic problem in the transformers, and the solutions that have been proposed by researchers. Harmonics problem in transformer is not new and has been previously reviewed from different point of views. Finite element analysis of distribution transformers under harmonics operation is reviewed in [10]. The application of optical sensors for monitoring transformer condition is discussed in [11], where classification of optical fiber sensors for transformer oil diagnostics is

also proposed. Methods developed for transformer derating due to non-linear loads are reviewed and compared in [7]. Their classification, advantages and disadvantages are also discussed. This thesis presents a comprehensive review of transformers supplying non-linear loads. The impacts, design, size optimization and derating are surveyed, orienting future researches towards the improvement of transformer efficiency and reliability. This review reveals that the major concern is the increase of ohmic and stray losses in the transformer which must be accurately calculated to improve the design of transformer by reducing these effects.

At the industrial design stage, it is very important to compute transformers stray losses caused by alternating electromagnetic field (EMF). This way, the derivation of new formulas is desirable sought to improve calculation and estimation methods. Several studies have been carried out recently with these objectives in mind [12], [13], [14]. Thus, analytical approaches have proven to be useful in calculating electromagnetic losses [12]. Generally speaking, there are two analytical methods to estimate eddy current (EC) losses in transformers tanks: (i) application of Poynting's theorem [15] and (ii) direct calculation of the EMF by solving Maxwell's equations [12]. In the first method (see Turowski's analytical method [15]), Poynting's theorem is used to estimate the power dissipation. However, the power dissipation formula contains semi-empirical parameters selected by non-rigorous methods. The precision of the second method is limited only by the difficulty of reproducing real geometries. In [16], axial component of the Electric Field (EF) in the tank wall was ignored while solving Maxwell's equations, which negatively impacted the accuracy of the obtained results [12].

In [12], analytical formulas for calculating EMF and EC losses in transformer tank walls were obtained by solving Maxwell's equations in the case of the axial geometry of the tank wall. The results demonstrated a good accuracy compared with the previous methods. However, a load

current with only the fundamental frequency was considered. Also, the obtained formulae involve Bessel functions, which might not be easily understood or commonly used in an industrial setting. None of the previously published works consider harmonics in the load current while deriving analytical models for computing losses in transformer tank walls.

Due to the increasing applications of non-linear loads, the computation of stray losses in transformer tanks requires the consideration of the harmonic content in the load current, with proper computation of the EMF. Therefore, it is of great importance to study the influence of the load current spectrum on the stray losses and heating of transformers. In this thesis, simplified analytical formulas to calculate the EMF and EC losses in the transformer tank wall are derived. The obtained formulas enable the analysis of the contribution of each harmonic to the power losses. Thus, it is a powerful and useful tool that can provide quick results in preliminary transformer designs without the need of expensive and high-end computational resources.

1.3 PROBLEM STATEMENT

Distortion in the load current has significant impacts on power transformers. It generates additional losses in the windings, core and structural parts of transformers. The contribution of stray losses in transformers cannot be ignored and must be studied and reviewed considering harmonics in the load current. Therefore, being economical and easy to implement, it is important to provide analytical solution for calculating stray losses in transformer, especially for the bushing regions which is perhaps one of the weakest part of power transformer. In this thesis, a comprehensive literature survey of the problem is presented and analytical expressions for calculating stray losses due to harmonics in transformer tank walls are obtained. Such study and analysis will improve the efficiency and reliability of the transformer.

1.4 HYPOTHESIS

The hypotheses of the thesis are as follows.

- In the literature, no comprehensive review has been presented that discusses harmonic problem in transformer and the solutions proposed for increasing transformer reliability.
- The computation of stray losses and EMF distribution considering harmonics using analytical approach should be based on solving Maxwell's equations in the geometry that represents most accurately the transformer tank wall.
- Harmonics in the load current, and its respective electric and magnetic fields, should be included by employing Fourier Series for computing stray losses in the tank walls.
- In the literature, no analytical expression has been presented for computing stray losses due to harmonics considering linear permeability of the tank wall.

1.5 OBJECTIVES

- General Objective

To present the literature survey of problems caused by distortions in voltage and current in transformers, and the solution proposed to minimize these problems. Additionally, to present analytical expressions for computing losses and EMF considering harmonics in the load current.

- Specific objectives
  - To carry out comprehensive literature survey of harmonic problems in transformers and the solutions proposed by researchers.
  - To obtain analytical expressions for computing EMF distribution and eddy current losses by solving Maxwell´s equations in transformer tank wall geometry.

- To validate the analytical expressions using 3-D Finite Element Method (FEM).
- To establish the experimental setup that can generate harmonic voltages and pass them through a transformer for evaluating their impacts on losses and temperature.

1.6 CONTRIBUTIONS

The contributions of the research work are as follows.

- An exhaustive literature survey that adequately categorizes the research works presented in the literature. The categorization includes the impacts of harmonics, proven actions for reducing harmonic impacts, and the state-of-the-art review of the popular techniques, derating and optimal sizing.
- Solving Maxwell's equations using appropriate boundary conditions in transformer tank wall geometry together with including harmonics in the load current.
- Obtaining electromagnetic models that represent transformer tank wall, separation of variable technique and asymptotic methods are used for the solution of Maxwell´s equations which allowed calculating EMF and obtain an analytical expression for losses calculation which considers harmonics in the load current.
- Verification of the obtained expressions using FEM software that validates their usefulness.
- With the obtained expressions, the losses and EMF distribution due to each harmonic can be evaluated and studied. These equations can be successfully employed in the industry to improve the design of the bushing regions.

- The experimental setup developed makes possible the generation of harmonic voltages and currents to pass them through a transformer to evaluate their impacts.

1.7 THESIS ORGANIZATION

The rest of the thesis is organized as follows. Chapter 2 presents the literature survey of the problem. It includes the mathematical models that are extensively used in literature for studying the harmonic impacts on transformers. Later, strategies that can be employed to tackle harmonic problem in the transformer are reviewed and discussed.

Chapter 3 presents the analytical formulation for studying harmonics effects in transformer tank walls. Several case studies have been carried out to evaluate losses in transformer tank wall due to harmonics.

Chapter 4 presents the simulations carried out using FEM software to validate the analytical expressions. FE simulations show close correspondence with the analytical results.

Chapter 5 is dedicated to the experimental work where controlling an Inverter for harmonics generation is explained. The Voltage containing harmonics are then passed through a transformer for impacts evaluation.

Finally, chapter 6 discusses the findings, conclusions, and future work that can be carried out to advance the subject.

Chapter 2. LITERATURE SURVEY

In this chapter, the losses due to harmonics in transformers and the approaches to reduce them are presented.

2.1 HARMONIC INDEXES

In this section, the commonly used indices for harmonics estimation are presented. The losses in the transformer due to non-linear loading depend upon the effective values, frequencies, and angles of the harmonic components.

In general, there are four methods for estimating harmonic load contents, i.e., crest factor, total harmonic distortion (THD), K-factor and harmonic load factor (F_{HL}). The most commonly used indices are the crest factor and percentage of THD. These two are adequate for knowing if the distortion in current or voltage has already occurred. The crest factor, which is the ratio between the waveform peak value and its true RMS value (see equation (2.1) below) is the simplest method for estimating harmonic load content [17]:

$$crest - factor = \frac{Peak}{RMS_{true}} \tag{2.1}$$

The concept behind the $crest - factor$ is that the deviation from $\sqrt{2} \approx 1.414$ implies distortion in the waveform. The second most popular method for harmonic and interharmonic content estimation, with a single number, is the THD. It is a measure of the effective harmonic

values as compared to the fundamental one. It can be mathematically represented as follows [18], [19]:

$$THD = \sqrt{\sum_{n=2}^{n}(I_n)^2} \Big/ I_1 \,, \tag{2.2a}$$

$$TIHD = \sqrt{\sum_{n=2}^{n}(I_k)^2} \Big/ I_1 \,, \tag{2.2b}$$

$$THD_{total} = \sqrt{THD^2 + TIHD^2} \,, \tag{2.2c}$$

where

THD : Total harmonic distortion.

$TIHD$: Total interharmonic distortion.

THD_{total} : Total harmonic and interharmonic distortion.

n : Harmonic.

k : Interharmonic.

Thus, THD is used to quantify the distortions in the current and voltage signals. The limiting value between high and low distortion levels is commonly 5 % [6], [20]. Both $crest - factor$ and THD are inadequate for transformers since they do not consider the frequency and harmonic angles.

Transformer losses are greatly dependent on the harmonic order of the distorted waveform. The sum of the squares of the harmonic load currents and the squares of the harmonic orders are factors that cause additional losses in the transformer. This important aspect is taken into account by the K-factor. It is defined as the summation of the squares of the p.u. harmonic currents times the square of the harmonic number, given in [17]:

$$K = \sum_{n=1}^{h} \left(I_{n(pu)}\right)^2 n^2 \tag{2.3}$$

where

$I_{n(pu)}$: Per unit harmonic current.

Another approach called F_{HL} for winding eddy current (WEC) and other stray losses are presented in an IEEE standard [21]. It represents the effective RMS heating due to distorted load current: the ratio between the total WEC losses, generated by harmonic currents, and the WEC losses at the fundamental frequency [21]. Similar to the K-factor, it does not account for the effect of the harmonic angles. F_{HL} is given by:

$$F_{HL} = \frac{P_{EC}}{P_{EC-O}} = \frac{\sum_{n=1}^{n=n_{max}} \left(\frac{I_n}{I_1}\right)^2 n^2}{\sum_{n=1}^{n=n_{max}} \left(\frac{I_n}{I_1}\right)^2} \tag{2.4}$$

where

F_{HL} : Harmonic loss factor.

P_{EC} : Winding eddy current losses.

P_{EC-O} : Winding eddy current losses at a fundamental frequency.

I_1 : The rms fundamental load current.

For computing stray losses in the structural parts of the transformer F_{HL} is obtained as:

$$F_{HL-STR} = \frac{\sum_{n=1}^{n=n_{max}} \left(\frac{I_n}{I_1}\right)^2 n^{0.8}}{\sum_{n=1}^{n=n_{max}} \left(\frac{I_n}{I_1}\right)^2} \tag{2.5}$$

where

F_{HL-STR} : Harmonic loss factor for stray losses in structural parts.

The relationship between F_{HL} and the K-factor is obtained from:

$$K = \sum_{n=1}^{n=n_{max}} \left(\frac{I_n}{I_1}\right)^2 F_{HL} \tag{2.6}$$

The use of F_{HL} is adequate for small conductors and lower order harmonics, leading to debatable results for large conductors and higher order harmonics [21]. Therefore, in [21] and [22] the following modified F_{HL} is obtained:

$$F_{HL} = \frac{\sum_{n=1}^{n=n_{max}} \frac{F(\xi_R) n^2 I_n^2}{F(\xi_R)}}{\sum_{n=1}^{n=n_{max}} I_n^2} = \frac{\frac{\sum_{n=1}^{n=n_{max}} F(\xi_n) n^2 I_n^2}{F(\xi_R) I^2}}{\sum_{n=1}^{n=n_{max}} \frac{I_n^2}{I^2}} \tag{2.7}$$

where

$F(\xi) = \frac{3}{\xi} \frac{\sinh \xi - \sin \xi}{\cosh \xi - \cos \xi}$, $\xi = \frac{T}{\delta}$ is the strand dimension related to the skin depth δ. It clearly takes account for the skin depth effect.

2.2 Modeling Impacts of Harmonics

Most of the previous research work has been aimed at investigating the impact of distortion on power losses, with a lesser focus on temperature rise and accelerated LOL. Total losses of distribution transformers in the European Union were estimated at about 38 TW · h/year, among which, the losses due to reactive power and harmonics were 5 TW · h/year [23].

Generally, the losses due to harmonics in the transformer are divided into two types, namely, no-load and load losses, as depicted in Figure 2.1. The former is due to the current flowing through the transformer, while the latter is continuous regardless of the load. No-load losses are subdivided into eddy current, hysteresis, and anomalous (or excess) losses. Eddy current losses occur due to the induced electromagnetic field (EMF) in the core caused by the alternating magnetic field. Hysteresis losses occur due to the reorientation of magnetic domains during each cycle of the alternating magnetizing force. Hence, the total core loss is a function of the voltage wave shape. Excess losses arise due to movement of domain walls, leading to the difference between measured and calculated eddy current losses. Load losses are categorized as ohmic and total stray losses. The former is generated by the conductor resistance, whereas the latter is subdivided into eddy current and other stray losses. Other stray losses are caused by leakage fluxes, which link the metallic parts of the transformer, such as the tank wall and clamping structure.

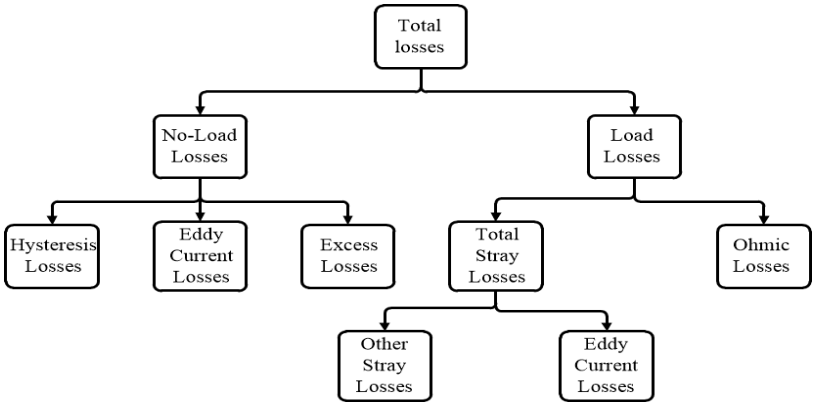

Figure 2.1: Transformer losses due to harmonics.

2.2.1 *Impacts of harmonic currents*

Distortion in the load current significantly increases the DC ohmic, WEC and other stray losses in transformers. IEEE standards [21] provides equations for calculating load losses. Copper losses rise with the square of the RMS harmonic currents as:

$$P_{ohmic} = R_{dc} \sum_{n=1}^{n_{max}} I_n^2 \tag{2.8}$$

where

P_{ohmic} : Ohmic losses.

R_{dc} : The dc resistance.

WEC losses are directly related to the square of the harmonic load currents and their orders:

$$P_{EC-non\,sin} = P_{EC-R} \left[\sum_{n=1}^{n_{max}} \left(\frac{I_n}{I_R} \right)^2 n^2 \right] \tag{2.9}$$

where

$P_{EC-non\,sin}$: Eddy current losses for non-sinusoidal load.

P_{EC-R} : Winding eddy current losses for rated load.

I_R : The rated current.

Other stray losses augment with the square of the harmonic load currents and their orders to the power 0.8:

$$P_{OSL-non\ sin} = P_{OSL-R}\left[\sum_{n=1}^{n_{max}}\left(\frac{I_n}{I_n}\right)^2 n^{0.8}\right] \quad (2.10)$$

where,

$P_{OSL-non\ sin}$: The non-sinusoidal other stray losses.

P_{OSL-R} : The other stray losses at rated load.

Although these equations give quick results, they have the following limitations and, therefore, lead to conservative results [21]:

1. They are reasonable for small conductors and lower order harmonics, giving conservative results for a large conductors and high order harmonics [21].
2. These equations do not consider skin-effect, influence of proximity or geometry, providing additional WEC losses [7], [2].

The skin depth can be considered using a modified F_{HL} in (7) [21] to obtain more accurate results. Ghazizadeh [2] et al. present an improved analytical method based on a finite-element approach, where each winding of the transformer is modelled considering skin, proximity, and geometric effects.

2.2.2 *Impacts of voltage harmonics*

Non-sinusoidal currents passing through the line and transformer impedances inject distortion to the supply voltage, which, in turn, deteriorates no-load operation, increasing power losses, temperature, noise, and LOL.

The EMF induced by an alternating flux is directly proportional to the flux density and frequency. The alternating current thus generated in the core depends inversely on the resistivity of the material, and directly on the thickness of the core. The eddy current losses in the core are

related to the square of the lamination thickness and the squares of the flux density and frequency. Eddy current losses in the core are proportional to the square of the magnetic flux density and frequency [24]:

$$P_{eddy} \propto B_{rms}^2 f^2 \tag{2.11}$$

where

P_{eddy} : Eddy current losses.

B_{rms}^2 : Rated affective flux density.

f : Frequency.

whereas hysteresis losses are proportional to the area of the hysteresis loop [25]:

$$P_h \propto f B_{rms}^2 \tag{2.12}$$

where

P_h : Hysteresis losses.

The excess loss, resulting from the domain walls movement, can be calculated using the following statistical approach [25]:

$$\frac{dW_A}{dt} = \left(\frac{GdbH_0}{\rho}\right)^{\frac{1}{2}} \left(\frac{dB}{dt}\right)^{\frac{3}{2}} \tag{2.13}$$

where

G : The damping effect of the eddy currents,

b : Width of the lamination.

d : Thickness of the lamination.

ρ : Resistivity of the lamination.

H_0 : The statistical distribution of the internal domain walls field.

2.2.3 *Impacts of Interharmonics*

IEEE task-force for the interhamonics [26] suggests that specific models for studying the impact of interharmonics on transformers need to be developed. Experimental results have shown that even very low amplitude subharmonics can saturate the core of a transformer [27], leading to additional losses, noise, temperature and RMS current increase [27].

Hysteresis loop asymmetrization and core saturation were studied in [28] under interharmonic operation. Load and no-load tests, carried out on a 1 kVA 230 V/24 V single phase transformer, have shown that subsynchronous interharmonic voltages increase significantly the RMS magnetizing current even with magnitudes less than 1 % of the fundamental. The effect depending on the ratio between magnitude and frequency. This can cause thermal and electromechanical stress, vibration and noise, which must be studied and modelled [28].

The impact of Interharmonics on a three-phase transformer were investigated in [29] by the same authors of [28]. Again, it was found that very low frequencies (from 1 to 5 Hz), even with low amplitudes, superimposed on the fundamental may saturate the core. The zero-sequence interharmonic effects on three-limb transformers are more severe as compared to the positive sequence, being independent of the rated power [29]. Their effects are independent of the rated power of the transformers [29]. Their impact on winding losses can be excessive, and therefore, must be taken into account while derating the transformer [30]. The impacts of harmonics and interharmonics on distribution transformers are summarized in Table 2.1.

Table 2.1: Impacts of harmonics and interhamonics on distribution transformer.

Transformer	Distortion profile	Study		Impacts	Reference
		Simulation method	Experimental		
3-φ, 50 kVA	THDi increase from 18.22 to (a) 23.01 % (b) 28.32 %	FEM	-	Eddy current losses increase from 100 W to (a) 120 W (b) 170 W	[8]
3-φ, 50 kVA	THDi of 37.33	FEM	-	Eddy current losses increase from 18.087 to 164.412 W	[2]
3-φ, 250 MVA	22 % of THDi	FEM and MATLAB	-	10 % increase in °C in top oil and 30 % increase in °C in hot spot	[31]
3-φ, 100 kVA	12 % THDi	FEM	-	Magnetic flux density increase by 9 % and losses increase by 7.8 %	[32]
Wound-core transformer	(a) 12.02 % of THDv line-to-line (b) 10.8 % of THDv line-to-neutral	FEM	Experimental verification	Deteriorate no-load operation by (a) 3.46 % (b) 1.51 %	[23]
3-φ, 5 kVA	(a) sinusoidal (b) 23 % THD (c) 36 % THD (d) 38 % THD	FEM	Experimental	(a) 76 W (b) 82 W (c) 85 W (d) 88 W	[3]
1-φ and 3-φ	Interharmonics 1 to 5 Hz	Numerical simulations	Experimental	Core saturation	[29]-[28]

2.2.4 *Impacts of typical non-linear loads*

Studies related to transformers subjected to typical non-linear loads are reviewed in this subsection. The THD_i generated by a single-phase welder, a personal computer, a three-phase six-pulse rectifier, a three-phase twelve-pulse rectifier, a three-phase induction furnace, and a three pulse DC arc furnace, is typically 31 %, 92 %, 26 %, 9 %, 27 %, and 22 %, respectively [33]. Regarding voltage harmonics, it is shown, for the network of a small Greek island, that the replacement of more than 30 % of CFLs over incandescent lamps can increase the THD_v by 8 %, while for bigger installations, the THD_v may reach 31 % [34].

The impacts of the typical non-linear loads on the distribution transformer are summarized in Table 2.2.

Table 2.2: Impacts of non-linear loads on the distribution transformer.

Transformer	Non-linear load	Study		Impacts	Ref
		Simulation Method	Experimental		
3-φ, 2 MVA	EV THDv=3.8 % THDi=24 %	PSPICE	Open and short circuit tests	6 % increase in losses	[35]
3-φ, 100 kVA	Solar panels	MATLAB	Experiments	Unbalance load and losses increase	[36]
3-φ, 5 MVA	Solar panels and associated PWM	MATLAB	Experiments	(a) Increase in temperature by 1.2 °C (b) decrease life by 8.3%	[37]
500 A	(a) LED loads (b) CFL	Thermal simulation study	Measurements using power quality analyzer	(a) 135.5 times increase in life time (b) 240 times increase in life time	[38]
3-φ, 2 MVA	(a) Less than 5 % distortion (b) sinusoidal + 6 pulse rectifier (c) sinusoidal + 12 pulse rectifier (d) rectifier + 10 % of 5^{th} harmonic	PSPICE	-	Loss of life (a) 1.1 % (b) 6% (c) 3.5 % (d) 7%	[39]
No given	Interharmonics 6 Hz, 14 Hz, 24 Hz (a) single-phase cycloconverter (b) three-phase cycloconverter	Matlab, PSPICE simulations	Experimental measurements	(a) *K*-factor increase by increasing the modulation index (b) *K*-factor decrease by increasing the modulation index	[19]

2.3 PROVEN DESIGN ACTIONS

Several design modifications can be carried out in order to decrease the effect of non-sinusoidal currents and voltages on distribution transformers. The acquisition of a transformer, subjected to non-linear loads, must include information of the harmonic spectrum of the load for appropriate transformer selection [40]. Otherwise, both the user and transformer designer are at technical and financial risk. Hence, steps must be taken in order to ensure an adequate design [21]. Several approaches have been suggested to deal with harmonics in transformers [40]: derating, oversizing, augmented insulation ratings and *K*-factor. However, the optimum method is subject to economic and technical factors [40].

2.3.1 *Proven actions at transformer design stage*

At the design stage, 1) the increase of primary windings for the reduction of the 3rd harmonic circulation, 2) the employment of improved magnetic core materials, 3) the connection to mitigate harmonics and 4) the use of transposed and isolated conductors are strategies that can be implemented by transformer manufacturers to reduce harmonic impacts [17], [41]. Improved permeability cores are useful in reducing other stray losses in magnetic shunts, tanks, and clamps [42], [43].

2.3.2 *IEEE recommendations*

IEEE recommends filtering harmonics at the secondary winding of the transformer [21] as an alternative to derating. However, filters must be carefully designed to avoid resonance. Electrostatic ground shields must be placed between the primary and secondary windings to reduce transients and line disturbances due to converter equipment [21]. Furthermore, non-

magnetic materials, blocking circulating currents, instead of mild steel and shielding materials, must be used in spacing zones [21].

2.3.3 *K-rated transformers*

There are special *K*-rated transformers [44], [45] that can supply power to harmonic loads within safe operating temperatures. They are more expensive than normal transformers because of their high capacity of power handling. They reduce eddy current losses and their effects, and comprise of designs ranging from *K*-1 to *K*-50 [4]. *K*-1 (indicates a linear load) is a standard for other *K* rating transformers. For example, *K*-9 has nine times higher handling capacity compared to *K*-1. Reference [46] suggests keeping a rigorous balance of ampere-turns between HV and LV windings to reduce radial components of the leakage flux and consequently stray losses in *K*-rated transformers.

2.3.4 *Transformer connections and configurations*

The main purpose behind the phase-shifting principle is to shift a phase via a transformer, cancelling harmonic components. This method displaces the phase of the current harmonic pairs by 180-degree by cancelling each other out. Positive sequence currents cancel negative ones, while zero sequence currents cancel each other [47]. Table 2.3 shows the angles required to cancel or attenuate the harmonics.

Table 2.3: Phase shift required for harmonic cancellation.

Harmonics	Phase shift
3^{rd}	60 degrees
5^{th} , 7^{th}	30 degrees
11^{th} , 13^{th}	15 degrees

2.4 TRANSFORMER SIZING AND DERATING

As stated earlier, the distortion in the load current and supply voltage increase transformer losses leading to an increase in the temperature, eventually, reaching the hot-spot [48]. Therefore, the transformer must be oversized or derated to compensate for harmonic impacts.

2.4.1 *Transformer sizing*

The presence of harmonics in the load current must be taken into account while computing the optimum transformer size. In [49], a new dynamic programming framework was proposed to solve the transformer optimal size problem under harmonic operation taking the following in consideration: excessive load losses, abnormal hottest-spot temperature rise, and depreciation cost variable. The authors recommend oversizing the transformer subjected to non-linear loads because the harmonic currents can significantly affect the optimal transformer size problem. For example, for the specific case of a distribution network in the city of Tehran, Iran, the authors found that 800 kVA transformer can be used for the first 19 years of service and then replaced it with a 1250 kVA one. As a result, initial 25% extra investment to design a low losses transformer (compared to an equivalent normal type) can be compensated by reducing total losses resulting in 20% lower total cost over its lifetime [49]. It is worth mentioning that the size increment of the transformer augments core losses, whereas the size decrement leads to more load losses and LOL [49].

2.4.2 *Transformer derating*

In harmonic regimes, a technique called derating is employed to limit the hotspot temperature within the permissible value [48]. Using this technique, the transformer is underutilized and the

temperature is prevented from exceeding the rated value, thus avoiding the accelerated LOL and eventually premature damage. However, the losses due to harmonics still persist in the transformer.

Two different approaches have been developed for derating transformers [7]. In the former, the no-load losses are ignored due to concern that the load current containing harmonics increases winding losses and temperature. The total load losses should not exceed the rated ones due to the fundamental and the harmonic components in the current. In the latter approach, the total losses due to sinusoidal and harmonic operation are considered as a lumped load while derating a transformer. Consequently, the transformer rating is reduced in such a way, making the losses identical of both linear and non-linear loading [7].

There are four individual methods developed for transformer derating, namely, IEEE recommended, analytical, experimental, and FEM. The latter is capable of estimating transformer losses with a high degree of accuracy making it the most recommended for transformer analysis and derating under harmonic operation. It is capable of including geometric effects, material properties, unbalanced condition, phase angles of distorted signals, and no-load operation in transformer loss estimation. The next favourable method is IEEE recommended because it is simple and quick for derating a transformer conservatively. However, it does not include unbalanced voltage condition, angles of harmonics, geometric effects, and no-load losses. The 3rd method is experimental. Both load and no-load losses can be estimated experimentally, however, the loss components cannot be obtained individually, and in the derating process, the most important factor is WEC losses. The least accurate method is analytical because it requires a lot of effort to include saturation effect, non-uniform flux

distribution, leakage fluxes, core lamination, thermal insulation properties, and the cooling effect [7].

When a transformer is subjected to non-linear loads with the unbalanced supply voltage, the copper and core losses increase and therefore, a mixed derating approach must be applied. The mixed derating approach can be applied to obtain a more approximated solution. In [50], a novel mixed derating approach was presented using 3-D TSFEM considering harmonic currents, an unbalanced supply voltage, and a 50 kVA transformer was derated. Under unbalanced supply voltage, the flux density is asymmetric and rises in the core. The computed power in kVA under 12 % and 23 % THD_i was 90.4 kVA and 87 kVA, respectively.

A 50 kVA distribution transformer was derated by computing F_{HL} using time stepping finite element method (TSFEM) in [8] under non-linear current and unbalanced supply voltage. Winding distribution, geometrical, and physical characteristics were all considered in the study. It was found that the mixed derating approach must be applied in cases where the load is non-linear and the supply voltage is unbalanced.

Taking advantage of the analytical method that can adequately consider skin effect, proximity effect, and geometric effect, it can be combined with FEM to obtain a more accurate solution. In [2], an improved analytical-FEM method is proposed by considering material characteristics, losses due to skin effect, proximity effect, and geometric effect. The losses in the core were not considered in the derating process since the voltage unbalanced was ignored.

Chapter 3. ANALYTICAL FORMULATION FOR COMPUTING TANK WALL LOSSES

3.1 INTRODUCTION

The conductor passing through the bushings and tank wall of a transformer is shown in Figure 3.1. The tank wall is considered as a disk of radius b with a hole of radius a in the center. An infinitely long conductor passes at a right angle through the hole. To avoid the complexity, the axial geometry of the system requires the use of the cylindrical coordinates for solving Maxwell's equations. Figure 3.2 shows the schematic geometry of the system which is divided into two regions. The hole, where the conductor is mounted, the medium above the tank wall, and the region below the wall are filled with air or any other dielectric. Region $R_I = \{(r,z): r_0 \leq r\} \backslash \{(r,z): a \leq r \leq b, |z| \leq h/2\}$, where r_0 and h are the conductor half diameter and the transformer tank thickness, respectively. Region $R_{II} = \{(r,z): a \leq r \leq b, |z| \leq h/2\}$ represents the tank wall, which is made up of a ferromagnetic material. In this work, the magnitude of the magnetic flux density is assumed such that the permeability of the tank wall can be considered constant.

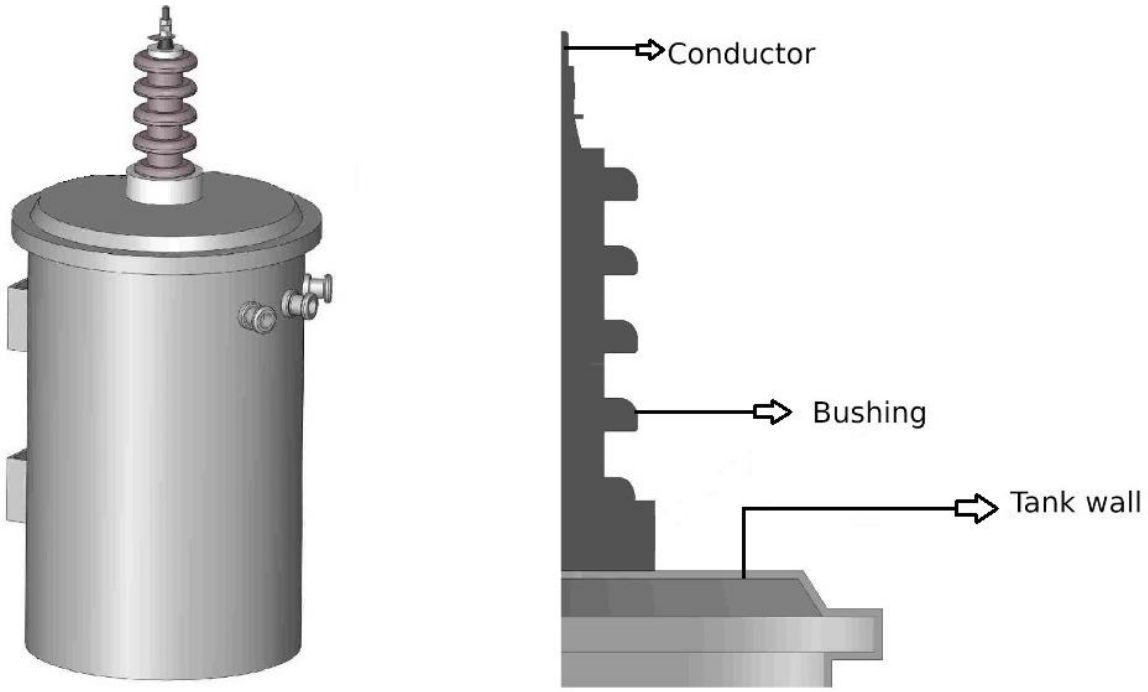

Figure 3.1: Conductor passing through the bushing regions of a transformer.

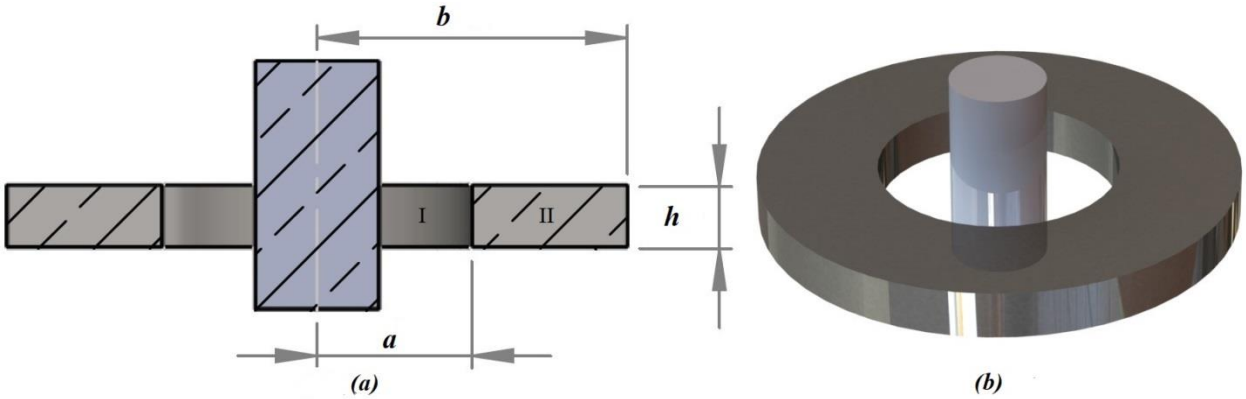

Figure 3.2: Tank wall geometry for calculating EMF.

3.2 MODELING EMF AND EDDY CURRENT IN THE TANK WALL

The conductor, passing through the hole, can be modeled as infinitely thin and long. With the advent of non-linear loads in the distribution system, the current carries an infinite number of harmonics:

$$I(t) = \sum_{n=-\infty}^{\infty} I_n e^{jn\omega t}, \tag{3.1}$$

where

ω : Fundamental angular frequency.

j : Imaginary number.

t : Time.

The EF and MF produced by the current-carrying conductor, in both regions can be expanded to a Fourier Series of the same form:

$$\mathbf{E} = \sum_{n=-\infty}^{\infty} \mathbf{E}_n e^{jn\omega t}, \tag{3.2}$$

$$\mathbf{H} = \sum_{n=-\infty}^{\infty} \mathbf{H}_n e^{jn\omega t}, \tag{3.3}$$

where

$\mathbf{E}_n$: Electric field.

$\mathbf{H}_n$: Magnetic field.

Because of the linear permeability of the tank wall, the complete system of Maxwell's equations in the quasi-static approximation can be written for each harmonic as follows:

$$\begin{aligned} \nabla \times \mathbf{E}_n &= -jn\omega\mu\mathbf{H}_n, & \nabla \cdot \mathbf{H}_n &= 0, \\ \nabla \times \mathbf{H}_n &= \mathbf{J}_n + \sigma\mathbf{E}_n, & \nabla \cdot \mathbf{E}_n &= 0, \end{aligned} \tag{3.4}$$

where

$\mathbf{J}_n$: Current density.

μ : Permeability.

σ : Conductance.

Because of the axial symmetry of the system, the solution to (3.4) can be sought as follows:

$$\mathbf{H}_n = H_{n,\varphi}(r,z)\mathbf{e}_\varphi, \qquad \mathbf{E}_n = E_{n,r}(r,z)\mathbf{e}_r + E_{n,z}(r,z)\mathbf{e}_z, \tag{3.5}$$

where the MF is an even function of the axial coordinate z: $H_{n,\varphi}(r,-z) = H_{n,\varphi}(r,z)$. System of equations (3.4) must be taken into account along with the boundary conditions given below in the interface of regions R_I and R_{II}.

$$\begin{aligned}
&H_{n,\varphi}^{(I)}\Big|_{r=a} = H_{n,\varphi}^{(II)}\Big|_{r=a}, \\
&\frac{\partial H_{n,\varphi}^{(I)}}{\partial z}\bigg|_{r=a} = \frac{\partial H_{n,\varphi}^{(II)}}{\partial z}\bigg|_{r=a} = 0, \\
&\frac{\partial H_{n,\varphi}^{(I)}}{\partial r}\bigg|_{r=a} = -\frac{H_{n,\varphi}^{(II)}}{a}\bigg|_{r=a},
\end{aligned} \tag{3.6}$$

$$\begin{aligned}
&H_{n,\varphi}^{(I)}\Big|_{r=b} = H_{n,\varphi}^{(II)}\Big|_{r=b}, \\
&\frac{\partial H_{n,\varphi}^{(I)}}{\partial z}\bigg|_{r=b} = \frac{\partial H_{n,\varphi}^{(II)}}{\partial z}\bigg|_{r=b} = 0, \\
&\frac{\partial H_{n,\varphi}^{(I)}}{\partial r}\bigg|_{r=b} = -\frac{H_{n,\varphi}^{(II)}}{b}\bigg|_{r=b},
\end{aligned} \tag{3.7}$$

$$\left.\frac{1}{r}\frac{\partial\left(rH_{n,\varphi}^{(I)}\right)}{\partial r}\right|_{z=\frac{h}{2}} = \left.\frac{1}{r}\frac{\partial\left(rH_{n,\varphi}^{(II)}\right)}{\partial r}\right|_{z=\frac{h}{2}} = 0,$$

$$\left.\frac{\partial H_{n,\varphi}^{(I)}}{\partial z}\right|_{z=\frac{h}{2}} = 0,$$

$$H_{n,\varphi}^{(I)}\Big|_{z=\frac{h}{2}} = H_{n,\varphi}^{(II)}\Big|_{z=\frac{h}{2}}, \tag{3.8}$$

3.3 EMF IN REGION R_I

The MF in air (Region I), according to the Ampere-Maxwell law, is:

$$H_{n,\varphi}^{(I)} = \frac{I_n}{2\pi r}. \tag{3.9}$$

Equation (3.9) implies that the MF magnitude does not depend upon φ or z and is inversely related to the distance from the conductor. Its direction is circumferential and therefore, the MF is circular around the conductor.

3.4 EMF IN REGION R_{II}

In region R_{II} system of equations (3.4) can be reduced to the following equation for the magnetic flux density:

$$\frac{1}{r}\frac{\partial}{\partial r}\left(r\frac{\partial H_{n,\varphi}^{(II)}}{\partial r}\right) + \frac{\partial^2 H_{n,\varphi}^{(II)}}{\partial z^2} - \frac{H_{n,\varphi}^{(II)}}{r^2} - jn\omega\mu\sigma H_{n,\varphi}^{(II)} = 0\,. \tag{3.10}$$

Equation (3.10) can be solved using the separation of variables technique [51]. As a result, the following expression is obtained:

$$H_{n,\varphi}^{(II)}(\mathrm{r},\mathrm{z}) = \left(\frac{A_n}{r} + B_n r\right)\cosh(\beta_n z) + \sum_{m=0}^{\infty}\left\{C_{n,m}I_1\left(\lambda_{n,m}r\right) + D_{n,m}K_1\left(\lambda_{n,m}r\right)\right\}\cos(k_m z) \quad (3.11)$$

where $I_1\left(\lambda_{n,m}r\right)$ and $K_1\left(\lambda_{n,m}r\right)$ are the modified Bessel functions of the first order, $\beta_n^2 = jn\omega\mu\sigma$, $k_m = \pi(2m+1)/h$ and $\lambda_{n,m}^2 = k_m^2 + \beta_n^2$, where $m = 0, 1, 2, \ldots$. In order to find the unknown constants $C_{n,m}$ and $D_{n,m}$, the boundary conditions (3.6) and (3.7) need to be applied. Therefore, we get:

$$\begin{cases} \beta_n\left(\frac{A_n}{a} + B_n a\right)\sinh(\beta_n z) - \sum_{m=0}^{\infty} k_m\left\{C_{n,m}I_1\left(\lambda_{n,m}a\right) + D_{n,m}K_1\left(\lambda_{n,m}a\right)\right\}\sin(k_m z) = 0, \\ \beta_n\left(\frac{A_n}{b} + B_n b\right)\sinh(\beta_n z) - \sum_{m=0}^{\infty} k_m\left\{C_{n,m}I_1\left(\lambda_{n,m}b\right) + D_{n,m}K_1\left(\lambda_{n,m}b\right)\right\}\sin(k_m z) = 0, \end{cases} \quad (3.12)$$

where $\sinh(\beta_n z)$ can be expanded in a Fourier series within the segment $z \in [-h/2, h/2]$ as follows (see [12]):

$$\sinh(\beta_n z) = \sum_{m=0}^{\infty} \frac{4\beta_n(-1)^m}{h\lambda_{n,m}^2}\cosh\left(\frac{\beta_n h}{2}\right)\sin(k_m z). \quad (13)$$

Substitution of (13) into the system of equations (12) yields:

$$\begin{cases} k_m\{C_{n,m}I_1(\lambda_{n,m}a) + D_{n,m}K_1(\lambda_{n,m}a)\} = \beta_n\left(\frac{A_n}{a} + B_n a\right)\frac{4\beta_n(-1)^m}{h\lambda_{n,m}^2}\cosh\left(\frac{\beta_n h}{2}\right), \\ k_m\{C_{n,m}I_1(\lambda_{n,m}b) + D_{n,m}K_1(\lambda_{n,m}b)\} = \beta_n\left(\frac{A_n}{b} + B_n b\right)\frac{4\beta_n(-1)^m}{h\lambda_{n,m}^2}\cosh\left(\frac{\beta_n h}{2}\right). \end{cases}$$

The solution to this system of equations (with respect to the constants $C_{n,m}$ and $D_{n,m}$) should be substituted into (9), resulting in the following solution to (10):

$$H_{n,\varphi}^{(II)}(\mathrm{r},\mathrm{z}) = \left(\frac{A_n}{r} + B_n r\right) + \sum_{m=0}^{\infty}\frac{4\beta_n^2(-1)^m}{hk_m\lambda_{n,m}^2}\frac{\cosh\left(\frac{\beta_n h}{2}\right)\cos(k_m z)}{I_1(\lambda_{n,m}a)K_1(\lambda_{n,m}b) - I_1(\lambda_{n,m}b)K_1(\lambda_{n,m}a)}$$
$$\times\left\{\left(\frac{A_n}{a} + B_n a\right)\left(I_1(\lambda_{n,m}r)K_1(\lambda_{n,m}b) - I_1(\lambda_{n,m}b)K_1(\lambda_{n,m}r)\right)\right.$$
$$\left.+\left(\frac{A_n}{b} + B_n b\right)\left(I_1(\lambda_{n,m}a)K_1(\lambda_{n,m}r) - I_1(\lambda_{n,m}r)K_1(\lambda_{n,m}a)\right)\right\}, \qquad (3.14)$$

where the constants A_n and B_n are to be found in the next section.

3.5 COUPLING OF EQUATIONS

Solutions (3.9) and (3.14) should be appropriately coupled by employing boundary conditions (3.6)-(3.8). First, taking into account that $\cos(k_m h/2) = 0$, the following result for the MF on the upper surface of the tank cover can be obtained from (3.14):

$$H_{n,\varphi}^{(II)}\left(r, \frac{h}{2}\right) = \left(\frac{A_n}{r} + B_n r\right)\cosh\left(\frac{\beta_n h}{2}\right). \qquad (3.15)$$

Substitution of (3.15) and (3.9) into boundary condition (3.8) yields:

$$\left(\frac{A_n}{r} + B_n r\right)\cosh\left(\frac{\beta_n h}{2}\right) = \frac{I_n}{2\pi r}. \tag{3.16}$$

Since the functions $1/r$ and r are linearly independent, the following solution for the constants A_n and $B_n$can be obtained:

$$A_n = \frac{I_n}{2\pi\cosh\left(\frac{\beta_n h}{2}\right)}, \quad B_n = 0.$$

Finally, substitution of these results into (3.14) yields the following solution to equation (3.10) in region R_{II}:

$$H_{n,\varphi}^{(II)}(r,z) = \frac{I_n}{2\pi r}\frac{\cosh(\beta_n z)}{\cosh\left(\frac{\beta_n h}{2}\right)} + \frac{I_n}{2\pi}\sum_{m=0}^{\infty}\frac{4\beta_n^2(-1)^m}{hk_m\lambda_{n,m}^2}\frac{\cos(k_m z)}{I_1(\lambda_{n,m}a)K_1(\lambda_{n,m}b) - I_1(\lambda_{n,m}b)K_1(\lambda_{n,m}a)}$$

$$\times\left\{\frac{1}{a}\left[I_1(\lambda_{n,m}r)K_1(\lambda_{n,m}b) - I_1(\lambda_{n,m}b)K_1(\lambda_{n,m}r)\right]\left[I_1(\lambda_{n,m}a)K_1(\lambda_{n,m}r)\right.\right.$$

$$\left.\left. - I_1(\lambda_{n,m}r)K_1(\lambda_{n,m}a)\right]\right\}. \tag{3.17}$$

Both equations (3.7) and (3.17) represent the solution to Maxwell's equations for the nth harmonic of the MF in the entire domain. The solution depends on the tank geometry (through the hole and disc radii *a* and *b*, the wall thickness *h*), amplitude of the nth harmonic of the

electric current and angular frequency (through the parameters $\lambda_{n,m}$ and β_n). It can be noticed that the dependence of the solution on the disc radius b can be neglected as shown below. According to (3.11), $\beta_n = (1+j)/\delta_n$, where $\delta_n = \sqrt{2/n\omega\mu\sigma}$ is the skin-effect depth for the nth harmonic of the MF. Therefore, the following estimation can be obtained:

$$\left|\lambda_{n,m}\right|^2 = \left|\left(\frac{\pi(2m+1)}{h}\right)^2 + \frac{2j}{\delta_n^2}\right| \geq \frac{2}{\delta_n^2}. \tag{3.18}$$

Therefore, $\left|\lambda_{n,m}\right| \geq \sqrt{2}/\delta_n$, which, due to smallness of the parameter δ_n, results in the estimation: $\left|\lambda_{n,m}b\right| \geq \sqrt{2}b/\delta_n \gg 1$. This estimation leads to the following asymptotic behavior of the modified Bessel functions [52]:

$$K_1\left(\lambda_{n,m}b\right) \propto \sqrt{\frac{\pi}{2\lambda_{n,m}b}}e^{-\lambda_{n,m}b} = \mathcal{O}\left(\sqrt{\frac{\delta_n}{b}}\, e^{-\frac{b}{\delta_n}}\right) \to 0 \;\; as \;\; \frac{b}{\delta_n} \to \infty, \tag{3.19}$$

where

$\mathcal{O}(\mathrm{x})$: The Landau big O notation [53].

Thus, the terms with $K_1\left(\lambda_{n,m}b\right)$ and $1/b$ in solution (3.17) can be neglected. As a result, the following equation is obtained:

$$H_{n,\varphi}^{(II)}(r,z) = \frac{I_n}{2\pi r}\frac{\cosh(\beta_n z)}{\cosh\left(\frac{\beta_n h}{2}\right)} + \frac{2\beta_n^2 I_n}{\pi a h}\sum_{m=0}^{\infty}\frac{(-1)^m}{k_m\lambda_{n,m}^2}\frac{K_1\left(\lambda_{n,m}r\right)}{K_1\left(\lambda_{n,m}a\right)}\cos(k_m z). \tag{3.20}$$

At the same time, if the hole radius a is much greater than the skin-effect depth δ_0 for the fundamental harmonic, i.e., $a \gg \delta_0$, then the following asymptotic formulas can be used for the functions $K_1(\lambda_{n,m}a)$ and $K_1(\lambda_{n,m}r)$, namely,

$$K_1(\lambda_{n,m}a) \propto \sqrt{\frac{\pi}{2\lambda_{n,m}a}}\, e^{-\lambda_{n,m}a} \quad and \quad K_1(\lambda_{n,m}r) \propto \sqrt{\frac{\pi}{2\lambda_{n,m}r}}\, e^{-\lambda_{n,m}r}. \tag{3.21}$$

Substitution of (3.21) into equation (3.20) results in the following approximate formula for the nth harmonic of the MF in the tank wall:

$$H_{n,\varphi}^{(II)}(r,z) = \frac{I_n}{2\pi r}\frac{\cosh(\beta_n z)}{\cosh\left(\frac{\beta_n h}{2}\right)} + \frac{2I_n\beta_n^2}{\pi h\sqrt{ar}}\sum_{m=0}^{\infty}\frac{(-1)^m}{k_m\lambda_{n,m}^2}\, e^{-\lambda_{n,m}(r-a)}\cos(k_m z). \tag{3.22}$$

Equation (3.22) is a simplified formula for computing MFs in tank walls of transformers. It does not require the use of special functions such as the modified Bessel functions, etc., which makes formula (3.22) simpler.

3.6 ELECTRIC FIELD (EF) AND EC LOSSES IN THE TANK WALL

Due to ohmic nature of EC losses, the average power density of losses can be expressed in the form:

$$P(\mathbf{r}) = \frac{1}{T}\int_0^T \sigma\mathbf{E^2}(\mathbf{r},\mathrm{t})dt, \tag{3.23}$$

where $\mathbf{E}(\mathbf{r},\mathrm{t})$ is the EF in region R_{II}, which can be obtained from Maxwell's equations (3.4) in the form:

$$\mathbf{E} = \frac{\nabla \times \mathbf{H}}{\sigma} = \sum_{n=-\infty}^{+\infty} \mathbf{E}_n e^{jn\omega t} = \sum_{n=-\infty}^{+\infty} \left(\mathbf{e}_r E_{n,r}(r,z) + \mathbf{e}_z E_{n,z}(r,z)\right) e^{jn\omega t}. \tag{3.24}$$

Substitution of (3.24) into (3.23) and accurate calculation of the respective integrals yields:

$$P(r,z) = \sum_{n=-\infty}^{+\infty} P_n(r,z),$$

where

$$P_n(r,z) = \frac{1}{2}\sigma\left(\left|E_{n,r}(r,z)\right|^2 + \left|E_{n,z}(r,z)\right|^2\right). \tag{3.25}$$

Here the radial component of the EF in the tank wall is:

$$E_{n,r}(r,z) = -\frac{1}{\sigma}\frac{\partial H_{n,\varphi}}{\partial z}$$

$$= -\frac{\beta_n I_n}{2\pi r\sigma}\frac{\sinh(\beta_n z)}{\cosh\left(\frac{\beta_n h}{2}\right)} + \frac{I_n}{2\pi\sigma}\sum_{m=0}^{\infty}\frac{4\beta_n^2(-1)^m}{h\lambda_{n,m}^2}\frac{\sin(k_m z)}{I_1(\lambda_{n,m}a)K_1(\lambda_{n,m}b) - I_1(\lambda_{n,m}b)K_1(\lambda_{n,m}a)}$$

$$\times\left\{\frac{1}{a}\left[I_1(\lambda_{n,m}r)K_1(\lambda_{n,m}b)-I_1(\lambda_{n,m}b)K_1(\lambda_{n,m}r)\right]\right.$$

$$\left.+\frac{1}{b}\left[I_1(\lambda_{n,m}a)K_1(\lambda_{n,m}r)-I_1(\lambda_{n,m}r)K_1(\lambda_{n,m}a)\right]\right\},$$

whereas the axial component takes the form:

$$E_{n,z}(r,z)=\frac{1}{\sigma}\frac{1}{r}\frac{\partial(rH_{n,\varphi})}{\partial r}=\frac{I_n}{2\pi\sigma}\sum_{m=0}^{\infty}\frac{4\beta_n^2(-1)^m}{hk_m\lambda_{n,m}}\frac{\cos(k_mz)}{I_1(\lambda_{n,m}a)K_1(\lambda_{n,m}b)-I_1(\lambda_{n,m}b)K_1(\lambda_{n,m}a)}$$

$$\times\left\{\frac{1}{a}\left[I_0(\lambda_{n,m}r)K_1(\lambda_{n,m}b)+I_1(\lambda_{n,m}b)K_0(\lambda_{n,m}r)\right]\right.$$

$$\left.-\frac{1}{b}\left[I_1(\lambda_{n,m}a)K_0(\lambda_{n,m}r)+I_0(\lambda_{n,m}r)K_1(\lambda_{n,m}a)\right]\right\}.$$

Using the same approximation as in (3.22), these components of the EF can be represented as follows:

$$\mathbf{E}_{n,r}(r,z)=-\frac{\beta_nI_n}{2\pi r\sigma}\frac{\sinh(\beta_nz)}{\cosh\left(\frac{\beta_nh}{2}\right)}+\frac{2\beta_n^2I_n}{\pi ah\sigma}\sum_{m=0}^{\infty}\frac{(-1)^m}{\lambda_{n,m}^2}\frac{K_1(\lambda_{n,m}r)}{K_1(\lambda_{n,m}a)}\sin(k_mz)$$

$$=\frac{2\beta_n^2I_n}{\pi ah\sigma}\sum_{m=0}^{\infty}\frac{(-1)^m}{\lambda_{n,m}^2}\left(\sqrt{\frac{a}{r}}e^{-\lambda_{n,m}(r-a)}-\frac{a}{r}\right)\sin(k_mz),\qquad(3.26)$$

$$E_{n,z}(r,z)=-\frac{2\beta_n^2I_n}{\pi ah\sigma}\sum_{m=0}^{\infty}\frac{(-1)^m}{k_m\lambda_{n,m}}\sqrt{\frac{a}{r}}e^{-\lambda_{n,m}(r-a)}\cos(k_mz),\qquad(3.27)$$

where expansion (3.13) of the function $\sinh(\beta_n z)$ in a Fourier series has been used.

By taking the integral of power density losses (3.23) over the whole conducting disk, the total losses in the tank wall can be computed. Thus, it can be written as:

$$P_{tot} = \int_a^{2\pi} d\varphi \int_a^b r dr \int_{-h/2}^{h/2} P(r,z) dz = 2\pi \sum_{n=-\infty}^{+\infty} \int_a^b r dr \int_{-h/2}^{h/2} P_n(r,z) dz$$

$$= \pi\sigma \sum_{n=-\infty}^{+\infty} \int_a^b r dr \int_{-h/2}^{h/2} \left(\left|E_{n,r}(r,z)\right|^2 + \left|E_{n,z}(r,z)\right|^2 \right) dz. \quad (3.28)$$

Results (3.26) and (3.27) for $E_{n,r}(r,z)$and $E_{n,z}(r,z)$ should be substituted into equation (3.28), where the integration over the variable z can be performed using the orthogonality of the system of functions $\{\sin(k_m z), \cos(k_n z)\}$. As a result, the following asymptotic expression for the total EC losses can be obtained:

$$P_{tot} \approx \sum_{n=-\infty}^{+\infty} \frac{2|\beta_n|^4 |I_n|^2}{\pi\sigma h a^2} \sum_{m=0}^{\infty} \frac{1}{\left|\lambda_{n,m}\right|^4} \int_a^b \left\{ \left| \sqrt{\frac{a}{r}} e^{-\lambda_{n,m}(r-a)} - \frac{a}{r} \right|^2 \right.$$

$$\left. + \frac{\left|\lambda_{n,m}\right|^2}{k_m^2} \frac{a}{r} e^{-2Re\{\lambda_{n,m}\}(r-a)} \right\} r dr$$

$$= \sum_{n=-\infty}^{+\infty} \frac{2|\beta_n|^4 |I_n|^2}{\pi\sigma h a} \sum_{m=0}^{\infty} \frac{1}{\left|\lambda_{n,m}\right|^4} \int_a^b \left\{ \frac{a}{r} + \left(1 + \frac{\left|\lambda_{n,m}\right|^2}{k_m^2}\right) e^{-2Re\{\lambda_{n,m}\}(r-a)} \right.$$

$$\left. - 2Re\left(\sqrt{\frac{a}{r}} e^{-\lambda_{n,m}(r-a)} \right) \right\} dr$$

$$= \sum_{n=-\infty}^{+\infty} \frac{2|\beta_n|^4 |I_n|^2}{\pi\sigma h a} \sum_{m=0}^{\infty} \frac{1}{\left|\lambda_{n,m}\right|^4} \left\{ a\, ln\frac{b}{a} + \frac{1 - e^{-2Re\{\lambda_{n,m}\}(b-a)}}{2Re\{\lambda_{n,m}\}} \left(1 + \frac{\left|\lambda_{n,m}\right|^2}{k_m^2}\right) \right.$$

$$\left. - 2Re\left(\sqrt{\frac{\pi a}{\lambda_{n,m}}}\, e^{\lambda_{n,m} a} \left[erf\left(\sqrt{\lambda_{n,m} b}\right) - erf\left(\sqrt{\lambda_{n,m} a}\right) \right] \right) \right\},$$

where $erf(x)$ is the error function [53]. Finally, taking advantage of the fact that the value of $\left|\sqrt{\lambda_{n,m} b}\right|$ is high we can approximately write: $erf\left(\sqrt{\lambda_{n,m} b}\right) \approx 1$. As a result, the following approximation can be suitably used for calculating the total losses:

$$P_{tot}$$

$$= \sum_{n=-\infty}^{+\infty} \frac{2|\beta_n|^4 |I_n|^2}{\pi\sigma h a} \left|\cosh\left(\frac{\beta_n h}{2}\right)\right|^2 \sum_{m=0}^{\infty} \frac{1}{\left|\lambda_{n,m}\right|^4} \left\{ a\, ln\frac{b}{a} + \frac{1}{2Re\{\lambda_{n,m}\}} \left(1 + \frac{\left|\lambda_{n,m}\right|^2}{k_m^2}\right) \right.$$

$$\left. - 2Re\left(\sqrt{\frac{\pi a}{\lambda_{n,m}}}\, e^{\lambda_{n,m} a}\, erfc\left(\sqrt{\lambda_{n,m} a}\right) \right) \right\}, \qquad (3.29)$$

where $erfc(x) = 1 - erf(x)$ is the complementary error function [53].

3.7 ANALYTICAL RESULTS

Figures 3.3 and 3.4 show the MF penetration in the transformer tank, computed for the first (60 Hz) and third harmonics (180 Hz) using formula (3.20) (Figures 3.3(a) and 3.4(a) for the first and Figures 4(b) and 5(b) for the third harmonics, respectively), for two different resistivities:

$\rho = 0.25 \times 10^{-6}\ \Omega \cdot \mathrm{m}$ in Figure 3.3 and $\rho = 0.75 \times 10^{-6}\ \Omega \cdot \mathrm{m}$ in Figure 3.4. In order to compare the MF distribution in the magnetic disk for different harmonic numbers, both harmonics were studied with the same value of the RMS current $I_{rms,1} = I_{rms,3} = 141.42$ A. In both cases the relative permeability was considered as $\mu_r = 200$. It can be observed in Figures 3.3 and 3.4 that the higher the harmonic number, the smaller is the penetration depth of the MF in the transformer tank.

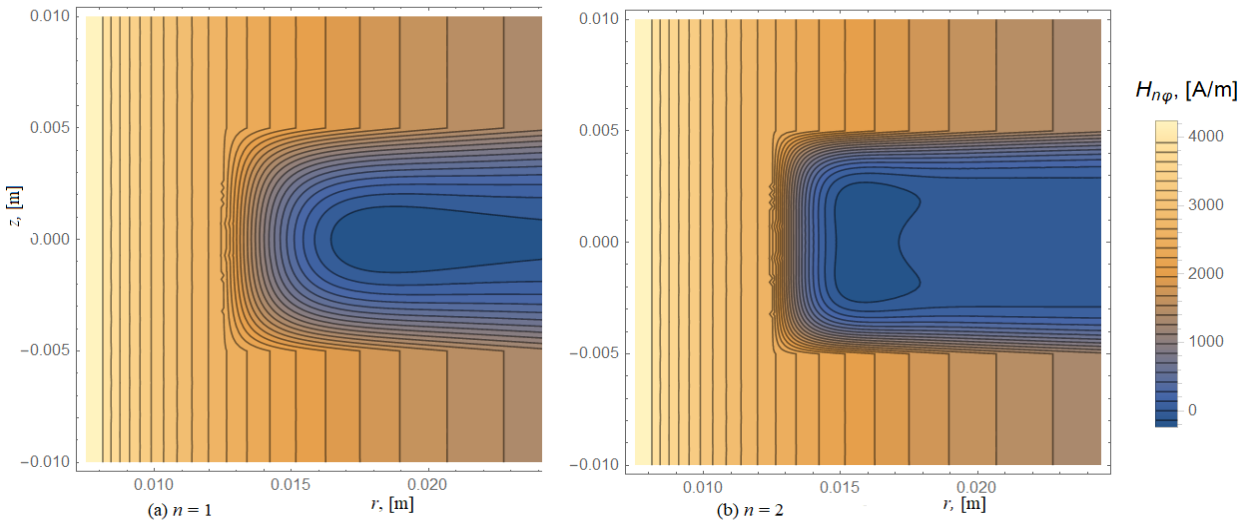

Figure 3.3: MF penetration in the transformer tank for $\rho = 0.25 \times 10^{-6}\ \Omega \cdot m$: (a) *n*=1, (b) *n*=3.

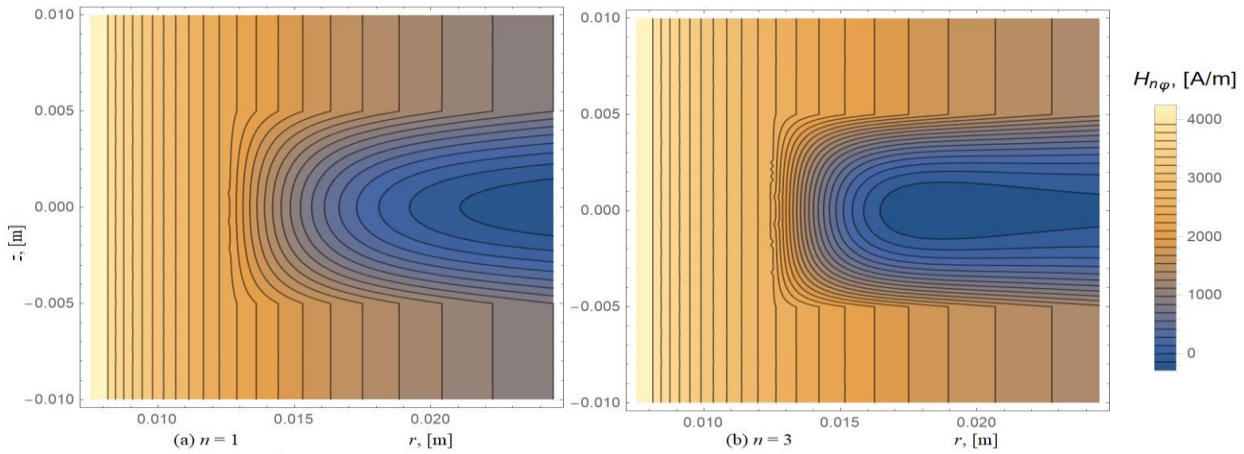

Figure 3.4: MF penetration in the transformer tank for $\rho = 0.75 \times 10^{-6}\ \Omega \cdot m$: (a) n=1, (b) n=3.

The EF distribution in the tank wall, computed using our analytical method (formulas (3.26) and (3.27)), is shown in Figures 3.5 and 3.6 for the first and third harmonics, under the same conditions (Figure 6 for $\rho = 0.25 \times 10^{-6}\ \Omega \cdot \mathrm{m}$ and Figure 3.6 for $\rho = 0.75 \times 10^{-6}\ \Omega \cdot \mathrm{m}$, also $I_{\mathrm{rms},1} = I_{\mathrm{rms},3} = 141.42$ A and $\mu_r = 200$ in both cases). Since the EC density is proportional to the EF ($j_n = \sigma E_n$), Figures 3.5 and 3.6 also qualitatively depict EC density lines in the tank wall. It can be observed that the ECs are mainly concentrated near the wall surface (skin-effect), and the concentration of the current density is higher for the third harmonic than for the first.

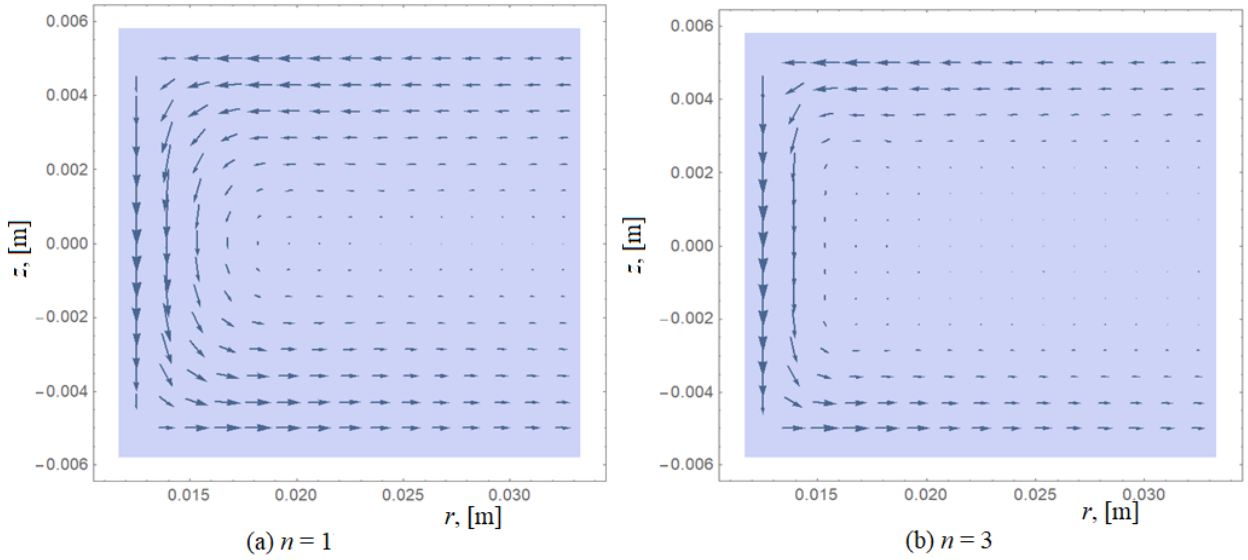

Figure 3.5: EF distribution in the transformer tank for $\rho = 0.25 \times 10^{-6}\ \Omega \cdot m$: (a) n=1, (b) n=3

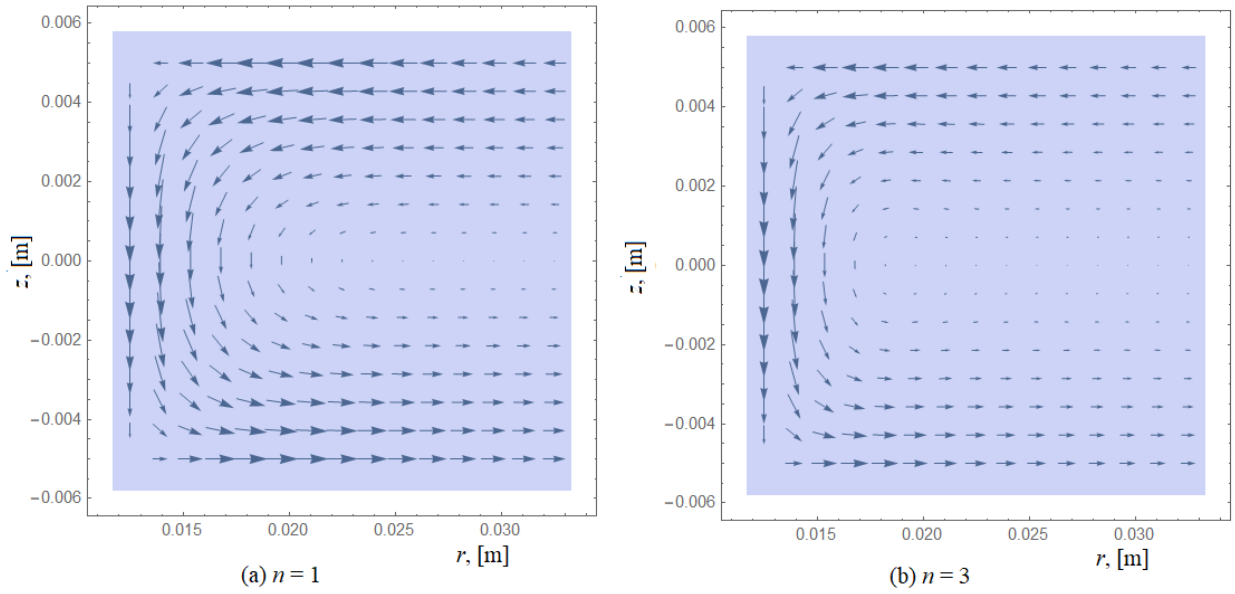

Figure 3.6: EF distribution in the transformer tank for $\rho = 0.75 \times 10^{-6}\ \Omega \cdot m$: (a) n=1, (b) n=3.

Chapter 4. VERIFICATION OF ANALYTICAL SOLUTION USING FEM

4.1 INTRODUCTION

From the literature survey presented in chapter 2, it is revealed that there are generally four methods for computing distortion impacts on transformers. They are FEM, analytical method, experimental method, and IEEE recommendations.

In order to verify the analytical model for transformer tank wall and provide a profound analysis of tank wall losses due to harmonics, FEM is used to simulate the behavior of the tank wall.

This method is widely used by designers at the industry and researchers due to its wide capacity to solve problems in electromagnetic devices, where the approximation to the models depends upon the parameters of the geometry and the material properties. Therefore, FEM software is commonly used for design validation, simulation of laboratory tests and failure analysis in transformers. This method is particularly useful in conditions where electromagnetic analysis is involved and that obtaining an acceptable solution via analytical method is difficult or impossible with the current knowledge. The advantages that FEM offers are as follows:

- It has the capability to handle complex geometries.
- It can properly include anisotropic, non-uniform, and non-linearity of the material.
- It has the capability to be coupled with circuits.

The fundamental equations that can model the eddy current losses are summarized in the following sections.

4.1 EMF MODELS

The transformer operating principle can be well studied by the Maxwell's equations. The fundamental equations that model the EMFs are the following Maxwell's equations:

$$\nabla \cdot \mathbf{D} = \rho \tag{4.1}$$

$$\nabla \cdot \mathbf{B} = 0 \tag{4.2}$$

$$\nabla \times \mathbf{E} = -\frac{\partial \mathbf{B}}{\partial t} \tag{4.3}$$

$$\nabla \times \mathbf{H} = \mathbf{J} + \frac{\partial \mathbf{D}}{\partial t} \tag{4.4}$$

where

B : The magnetic field density.

D : The electric flux density.

The continuity equation is as follows:

$$\nabla \cdot \mathbf{J} = -\frac{\partial \mathbf{D}}{\partial t} \tag{4.5}$$

The relationships of magnetic field density with MF strength, current density with EF strength, and electric flux density with EF strength are as follows:

$$\mathbf{B} = \mu\mathbf{H} = \mu_0\mu_r\mathbf{H} \tag{4.6}$$

$$\mathbf{J} = \sigma\mathbf{E} \tag{4.7}$$

$$\mathbf{D} = \varepsilon\mathbf{E} = \varepsilon_0\varepsilon_r\mathbf{E} \tag{4.8}$$

where

ε : The electric permittivity.

ε_0 : The permittivity in vacuum.

ε_r : The relative permittivity.

μ : The permeability.

μ_0 : The permeability in vacuum.

μ_r : The relative permeability.

σ : The electric conductivity.

4.2 Electric Scaler Potential

Charges at rest produce no current and MF, mathematically, can be written as follows,

$$\nabla \cdot \mathbf{E} = 0 \tag{4.9}$$

A scaler electric potential, represented by *V*, can be related with E as follows,

$$\mathbf{E} = -\nabla V \tag{4.10}$$

where

V : The scaler electric potential.

Equation (4.10) agrees with equation (4.9) since the curl of the gradient of a variable is always zero. Therefore, first equation of Maxwell (equation 4.1) takes the form,

$$\nabla \cdot \varepsilon \mathbf{E} = \rho_v \Rightarrow \nabla \cdot \varepsilon(-\nabla V) = \rho_v \tag{4.11}$$

or

$$\frac{\partial}{\partial x}\varepsilon_x \frac{\partial V}{\partial x} + \frac{\partial}{\partial y}\varepsilon_y \frac{\partial V}{\partial y} + \frac{\partial}{\partial z}\varepsilon_z \frac{\partial V}{\partial z} = -\rho_v \tag{4.12}$$

where

ρ_v : Electric charge density.

For homogeneous and isotropic materials, $\varepsilon_x = \varepsilon_y = \varepsilon_z = \varepsilon$, equation (4.12) takes the form given below,

$$\frac{\partial^2 V}{\partial x^2} + \frac{\partial^2 V}{\partial y^2} + \frac{\partial^2 V}{\partial z^2} = -\frac{\rho_v}{\varepsilon} \tag{4.13}$$

Or

$$\nabla^2 V = -\frac{\rho_v}{\varepsilon} \tag{4.14}$$

Equation (4.14) is also called poisson's equation governing electrostatic field distribution.

4.3 MAGNETIC VECTOR POTENTIAL

Magnetic vector potential is commonly used for 2-D MF problems. It is represented by vector **A**. It can be understand from equation 4.2 that, as the divergence of curl of any vector gives a result zero, therefore, the vector **B** can be expressed as the curl of another vector, as follows,

$$\mathbf{B} = \nabla \times \mathbf{A} \tag{4.15}$$

where

A : Magnetic vector potential.

Using the above expression together with Biot-Savart law for the magnetic flux density, the following expression for magnetic vector potential at a point due to volume current distribution as [54],

$$A = \int_v \frac{\mu_0 \, \mathbf{J} \, dv}{4\pi R} \tag{4.16}$$

where

R : The distance of the point from elemental volume.

4.4 MAGNETIC SCALER POTENTIAL

To solve problems requiring high computational burden, especially for complex 3-D problems, magnetic scaler potential can be used. However, magnetic scaler potential cannot be applied to the problems that involve current sources. Therefore, a reduced scaler potential-based formulation can be employed for the magnetostatic fields. This formulation is based on the sum of two components, (i) current distribution in the domain, (ii) other representing the remaining field [54].

$$\mathbf{H} = \mathbf{H}_c + \mathbf{H}_m \tag{4.17}$$

where $\mathbf{H}_c$ (the current distribution), can be defined as,

$$\nabla \times \mathbf{H}_c = \mathbf{J} \tag{4.18}$$

This current can be determined integrating directly using Biot-Savart Law. The curl free field ($\mathbf{H}_m$**)** can be defined in terms of reduced magnetic scalar potential **(**Ω_r **)** as follows,

$$\mathbf{H}_m = -\nabla\Omega_r \tag{4.19}$$

Equation (4.11) becomes,

$$\mathbf{H} = \mathbf{H}_c - \nabla\Omega_r \tag{4.20}$$

where Ω is the total scaler potential.

4.5 MIXED POTENTIAL APPROACH

The magnetic vector potential can be applied to steady state problems. The domain of study can be divided into two parts, (i) conducting region with eddy currents, and (ii) non-conducting region. In the former case, the scaler potential (V) need to be solved together with magnetic vector potential **A**. In the latter case, only magnetic vector potential is solved.

The **A**-V and **A** formulations for the aforementioned region are as follows:

(i) Eddy current regions: The potentials used are $-A_x$, A_y, A_z, and V.

(ii)

$$\nabla \times \frac{1}{\mu} \times \mathbf{A} + \sigma \nabla V + \sigma \frac{\partial \mathbf{A}}{\partial t} = 0 \tag{4.21}$$

$$\nabla \cdot \left(-\sigma \nabla V - \sigma \frac{\partial \mathbf{A}}{\partial t} \right) = 0 \tag{4.22}$$

(iii) Non-conducting regions: The potentials used are: $-A_x$, A_y, and A_z.

(iv)

$$\nabla \times \frac{1}{\mu} \nabla \times \mathbf{A} = 0 \tag{4.23}$$

For eddy current regions, there are two equations since the unknowns are two i.e. **A** and V. These equations can be employed in multiply connected regions. They are also applicable in cases where external circuits are coupled. However, these formulations lead to a large number of unknowns in 3-D applications. Therefore, **T**- Ω formulations have been proposed for computing eddy currents in transformers. In the conducting regions having eddy currents, this formulation requires only one or two components of **T**. In the non-conducting regions, the value of **T** is zero.

It is worth mentioning that the **T**- Ω formulations are particularly suitable for laminated regions such as core and tank walls [55]-[56].

4.6 CURRENT VECTOR POTENTIAL FOR 3-D EDDY CURRENTS

Other way to solve 3-D eddy current problem is the current vector potential. It can be achieved by obtaining the current density from current vector potential **T** [57].

$$\mathbf{J} = \nabla \times \mathbf{T} \tag{4.24}$$

From Ampere´s law, the following expressions can be obtained:

$$\nabla \times \mathbf{H} = \nabla \times \mathbf{T} \tag{4.25}$$

$$\mathbf{H} = \mathbf{J} - \nabla \emptyset_T \tag{4.26}$$

where

$\emptyset_T$: General magnetic scaler potential.

By comparing $\mathbf{H} = \mathbf{H}_s - \nabla\emptyset$ with the equation (4.26), and calculating **T** from Biot-Savart's law, in such a case, T can be replaced by $\mathbf{T}_0$. When both massive and filamentary conductors exist together, the expression for MF becomes [58]:

$$\mathbf{H} = \mathbf{T}_e + \mathbf{T}_0 - \nabla \emptyset_T \tag{4.27}$$

where $\mathbf{T}_e$ is used for massive conductors. Consequently, the Ampere´s law takes the form:

$$\mathbf{J} = \nabla \times \mathbf{T}_e + \nabla \times \mathbf{T}_0 \tag{4.28}$$

By substituting equations (4.27) and (4.28) in Faraday's law, we get,

$$\nabla \times \frac{1}{\sigma} \nabla \times \mathbf{T}_e + \frac{\partial}{\partial t} \mu \mathbf{T}_e = -\frac{\partial}{\partial t} \mu (\mathbf{T}_0 - \nabla \emptyset_T) - \nabla \times \frac{1}{\sigma} \nabla \times \mathbf{T}_0 \tag{4.29}$$

The solenoid property of **B** is as follows,

$$\nabla \cdot \mu (\mathbf{T}_e - \nabla \emptyset_T) = -\nabla \cdot \mu \mathbf{T}_0 \tag{4.30}$$

Equations (4.29) and (4.30) can be combined by taking the divergence.

4.7 FEM TANK WALL MESHING

66212 volume finite elements, 14992 surface elements, and 1292 line elements were used to mesh the geometry, which gave as a result a total number of 82496 elements. Also, to properly simulate the skin-effect in a thin boundary layer of the disk and to ensure a better accuracy of computations, nine layers of FE mesh of 0.255 mm of height each one, were generated near the upper surface of the disk as shown in Figure 4.1 (a). Additionally, a high-density mesh was created near the conductor (see Figure 4.1 (b)).

A disk with the characteristics: $h = 0.010$ m, $a = 0.0125$ m, $b = 0.150$ m, and $\varepsilon_r = 1$ is considered. A copper conductor with a radius $r_0 = 2$ mm and length 1400 mm crosses the disk at the center of the hole. One quarter of the entire disc and a half of its height were considered in the simulations, taking advantage of the symmetry of the problem. The total system was enclosed in a cylinder with an inner radius of 255 mm, an outer radius of 305 mm, an inner half height of 700 mm and an outer half height of 800 mm, as shown in Figure 4.2.

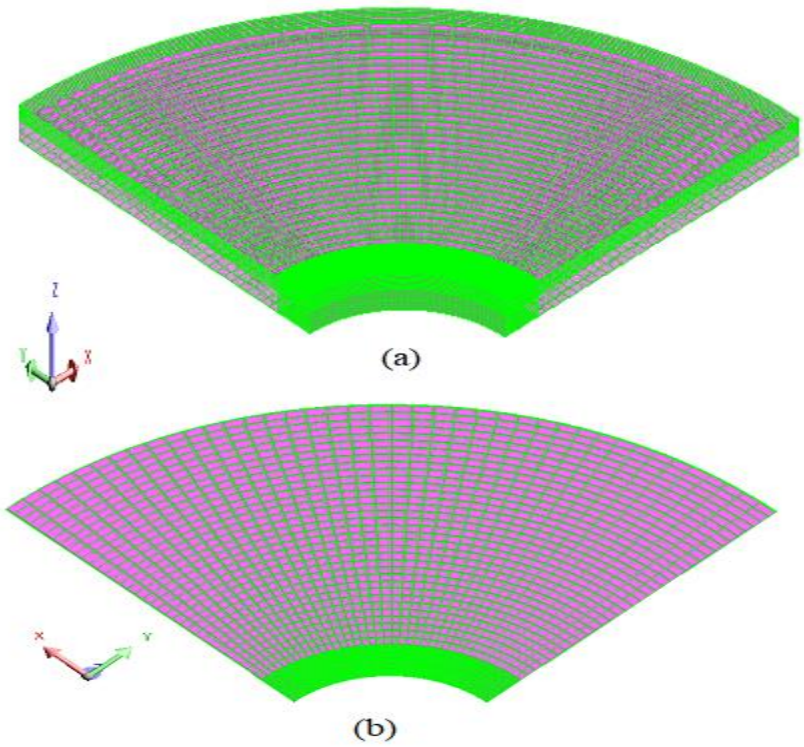

Figure 4.1: Finite element mesh: (a) 3-D view (b) top view

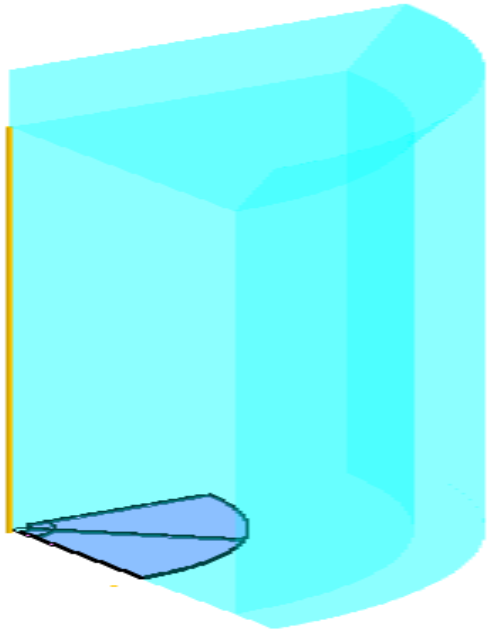

Figure 4.2: FE tank model enclosed in infinite box.

4.8 FEM RESULTS AND COMPARISON WITH ANALYTICAL MODEL

Several simulations were carried out in order to compare the analytical results with FEM solutions. FEM computations were carried out using Altair Flux finite element (FE) software.

Figures 4.3 and 4.4 show the FEM-calculated magnetic flux density distribution in the transformer tank for $\rho = 0.25 \times 10^{-6}\ \Omega \cdot \mathrm{m}$ and RMS current $I_{\mathrm{rms}} = 141.42$ A for the first and third harmonics, respectively. The maximum value of the magnetic flux density $B = 637.94 \times 10^{-3}$ T was obtained on the hole surface for the first harmonic (see Figure 4.3, whereas for the third harmonic it was $B = 638.19 \times 10^{-3}$ T (Figure 4.4).

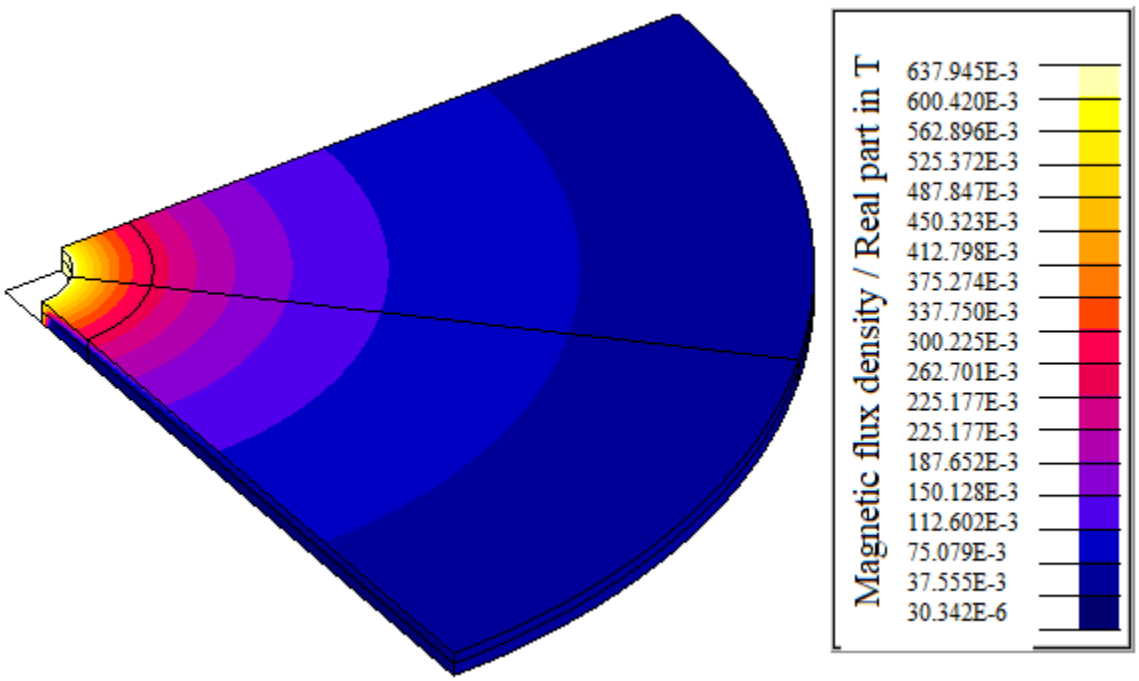

Figure 4.3: Magnetic flux density distribution in transformer tank wall for $\rho = 0.25 \times 10^{-6}\ \Omega \cdot \mathrm{m}$: for *n*=1.

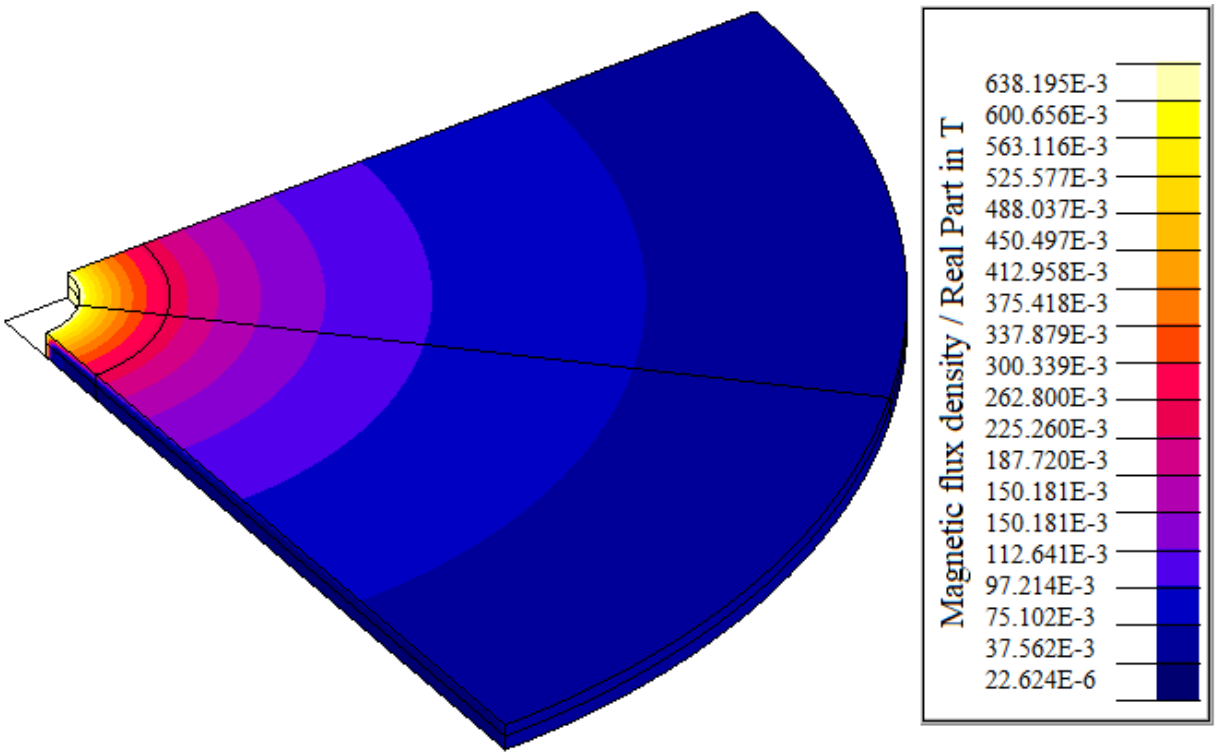

Figure 4.4: Magnetic flux density distribution in transformer tank wall for $\rho = 0.25 \times 10^{-6}\ \Omega \cdot \mathrm{m}$: for *n*=3.

The absolute value wave-form for the MF on the central plane of the tank wall (at z=0) is shown in Figures 4.5 and 4.6, where the blue line represents the analytical solution and the red points correspond to FEM simulations. Figure 4.5 is plotted for a resistivity $\rho = 0.25 \times 10^{-6}\ \Omega \cdot m$, whereas Figure 4.6 shows the MF profile for $\rho = 0.75 \times 10^{-6}\ \Omega \cdot \mathrm{m}$. Figures 4.5 and 4.6 show an excellent match between the analytical and FEM computations, which validates (3.22)–(3.26). On the other hand, the time taken while executing the analytical model was 0.66 seconds which is notably less than several minutes FE software takes in execution.

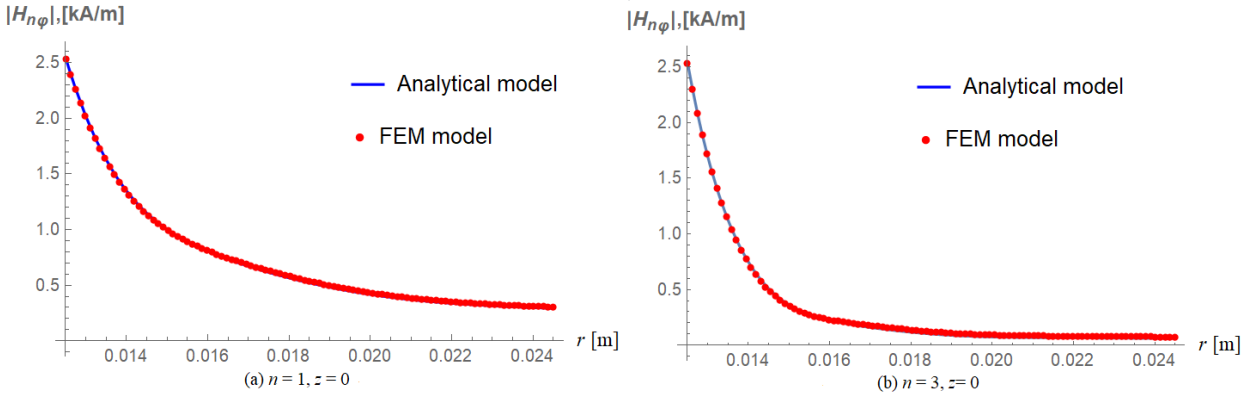

Figure 4.5: MF intensity in the mid-plane of the transformer tank for $\rho = 0.25 \times 10^{-6}\ \Omega \cdot \mathrm{m}$: (a) n=1, (b) n=3.

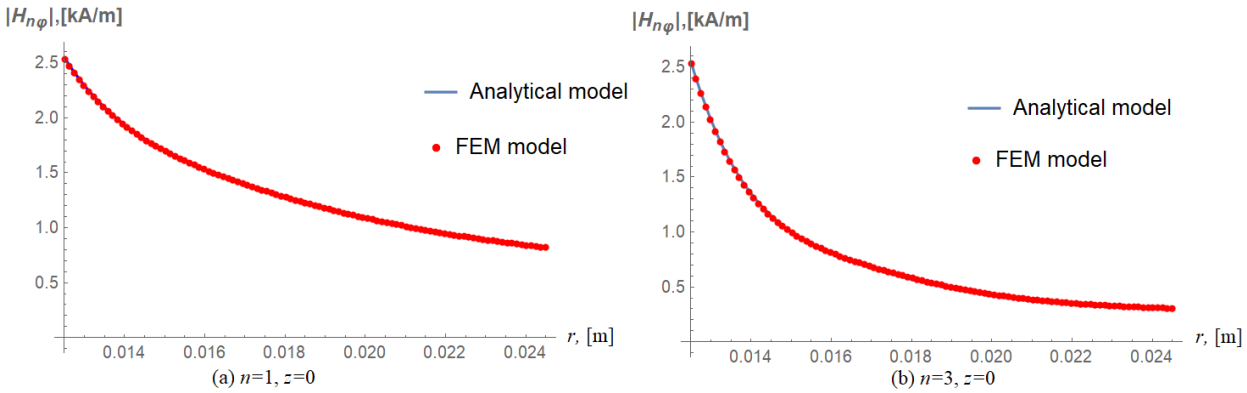

Figure 4.6: MF intensity in the mid-plane of the transformer tank for $\rho = 0.75 \times 10^{-6}\ \Omega \cdot \mathrm{m}$: (a) n=1, (b) n=3.

To validate formula (4.29), total EC losses were analytically and numerically computed for 8 different cases, where the radii, resistivity, and frequency were varied (see Table 4.1). Results of simulations are presented in Table 4.2. From table 4.2, it can be observed that both the analytical and FEM-calculated results are very close. The relative error between analytical and FEM solutions is in the range 0.13% to 1.610%, which proves the high accuracy of formulas (4.26), (4.27) and (4.29). Moreover, although the skin-effect depth decreases for higher frequencies, the MF density in the surface layer increases, which leads to higher losses.

Table 4.1: Transformer tank parameters and frequencies of the 8 cases studied ($\mu_r = 200$).

Case	*a*, [m]	*b*,[m]	*h*, [m]	*Irms*, [A]	ρ, [$\Omega \cdot$ m]	Harmonic
1	0.0125	0.150	0.010	141.42	0.25×10^{-6}	n =1
2	0.0125	0.150	0.010	141.42	0.25×10^{-6}	n =3
3	0.04	0.145	0.00952	141.42	0.25×10^{-6}	n =1
4	0.04	0.145	0.00952	141.42	0.25×10^{-6}	n =3
5	0.04	0.145	0.00952	141.42	0.25×10^{-6}	n =5
6	0.035	0.140	0.00952	141.42	0.75×10^{-6}	n =1
7	0.035	0.140	0.00952	141.42	0.75×10^{-6}	n =3
8	0.035	0.140	0.00952	141.42	0.75×10^{-6}	n =5

Table 4.2: Total stray losses in the disk for the 8 cases ($\mu_r = 200$).

Case	Ptotal [W], Analytical	Ptotal [W], Numerical	Relative error (%)	Skin depth, [mm]	Harmonic
1	1.874	1.870	0.22	2.297	*n* =1
2	3.276	3.267	0.27	1.326	*n* =3
3	0.959	0.953	0.63	2.297	*n* =1
4	1.632	1.630	0.13	1.326	*n* =3
5	2.127	2.117	0.47	1.027	*n* =5
6	1.614	1.588	1.61	3.979	*n* =1
7	3.108	3.100	0.26	2.297	*n* =3
8	3.917	3.901	0.41	1.779	*n* =5

Chapter 5. HARMONIC IMPACTS ON TRANSFORMER: EXPERIMENTAL WORK

In this chapter, the experimental work done during PhD studies has been explained. The progress on the research work in laboratory was postponed due to COVID-19 pandemic, therefore the work has not been completed. The work intended to study the impacts of harmonics and interharmonics voltages on transformer.

In this work, an experimental setup is established that allows generating (non)sinusoidal voltages. The distorted voltages are then passed through a transformer connected to its nominal load. The transformer losses due to each harmonic component are analyzed and temperature is monitored using RTD sensor.

5.1 VOLTAGE SOURCE CONVERTER FOR VOLTAGE TRACKING

A voltage source based on power converter together with an LC filter is considered for voltage tracking for this research work. Figure 5.1 shows the inverter connected to LC filter and transformer. The setup consists of a power inverter which is controlled to give a desired output voltage. A low pass LC filter is connected at the output of the inverter to remove the undesirable harmonics generated by switching effect from the voltage signal. The aim is to obtain i_{HuT} as close as possible to the reference of the inverter. The filtered voltage is applied to a single phase, 200 VA transformer that steps down 125 V to 24 V. A resistive load of 2.8 ohms is connected at the secondary of the transformer to withdraw the nominal current of the transformer i.e. 8.3 A. The purpose of the proposed setup is to operate transformer at its nominal voltages and currents and pass harmonics through it to investigate their impacts such as losses and temperature.

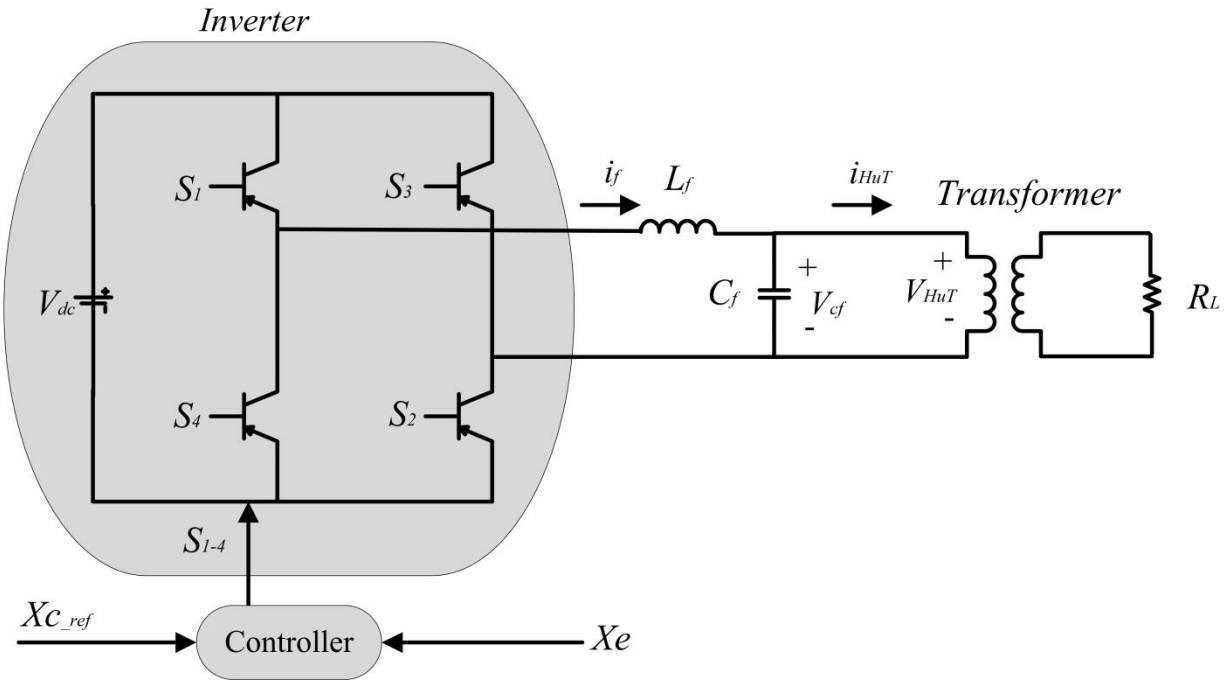

Figure 5.1: Schematic diagram of the experiment setup established.

The success of the scheme is subject to the voltage tracking of the closed loop control system. The control system contains a triangular signal and a sample having frequency of $1/\mathrm{T_s}$. The structure is shown in Figure 5.2, where x_c and x_{cref} are the state vectors, respectively. The error vector thus obtained is multiplied by the gain matrix $-K$. The reference voltage $v_{virtual}$ is utilized as a feedforward term where a constant η of it is added to obtain u_c (see Figure 5.2). The signal obtained is then compared with the triangular carrier to generate switching signal. Switches S_1 to S_4 are finally turned ON and OFF to get the output signal for filtering. The control law is given as follows [59]:

$$u_c(k) = -K_c\left[x_c(k) - x_{cref}(k)\right] + \eta$$

$$v_{virtual}(k) = -[k_1\ k_2] * \left[u_c(k) - x_{cref}(k)\right] + \eta v_{virtual}(k), \qquad (5.1)$$

where

K_c : Control constants.

x_{cref} : reference signal.

$v_{virtual}$: virtual voltage

η : Control constant.

The reference signal, $x_{cref} = [0\ v_{virtual}]$ and the states are given by $x_c = \left[i_f\ v_{cf}\right]$. Referring to the figure 5.2, a state vector, $x = \left[i_f\ v_{cf}\right]$ is established. The state space equation for the filter circuit is given below [59]:

$$A = \begin{bmatrix} 0 & -\frac{1}{L_f} \\ \frac{1}{C_f} & 0 \end{bmatrix}, B = \begin{bmatrix} \frac{V_{dc}}{L_f} \\ 0 \end{bmatrix} \tag{5.2}$$

where

L_f : Filter inductance.

C_f : Filter capacitance.

V_{dc} : dc voltage.

The reference for the capacitor voltage v_{cf} is given by $v_{virtual}$. Nevertheless, the reference for the current i_f is not directly available. The extended vector formed for the entire network is given below [59]:

$$x_e = [i_f \quad v_{cf} \quad i_{HuT} \quad i_{fLP}]$$

i_f : Current in the inductor.

v_{cf} : Voltage in the inductor.

i_{HuT} : Current hardware under test.

The equations of current and voltage in the filter are as follows:

$$i_{fHP} = i_f - i_{fLP} \tag{5.3}$$

$$v_{cfHP} = v_{cf} - v_{cfLP} \tag{5.4}$$

where

$$i_{fLP} = \frac{\alpha}{s+\alpha} i_f \tag{5.5}$$

$$v_{cLP} = \frac{\alpha}{s+\alpha} v_{cf} \tag{5.6}$$

$$A_e = \begin{bmatrix} 0 & -\frac{1}{L_f} & 0 & 0 \\ \frac{1}{C_f} & 0 & -\frac{1}{C_f} & 0 \\ 0 & \frac{1}{L_{eq}} & -\frac{R_{eq}}{L_{eq}} & 0 \\ \alpha & 0 & 0 & -\alpha \end{bmatrix}, B_e = \begin{bmatrix} \frac{V_{dc}}{L_f} \\ 0 \\ 0 \\ 0 \end{bmatrix},$$

where $Z_{eq} = R_{eq} + j\omega L_{eq}$ is the equivalent impedance of the transformer and the load connected at the secondary of the transformer. The control law obtained in [59] is given as follows:

$$u_c(k) = k_1\left[i_{f1HP}(k) - 0\right] - k_2\left[v_{cf}(k) - v_{virtual}(k)\right] + \eta v_{virtual}(k) = -K_e x_e(k) + (k_2 + \eta)v_{virtual}(k), \quad (5.7)$$

where $K_e = [k_1 \quad k_2 \quad 0 \quad -k_1]$. The closed loop system is then given by the following equation [59]:

$$x_e(k+1) = (F_e - G_e K_e)x_e(k) + (k_2 + \eta)v_{virtual}(k) \quad (5.8)$$

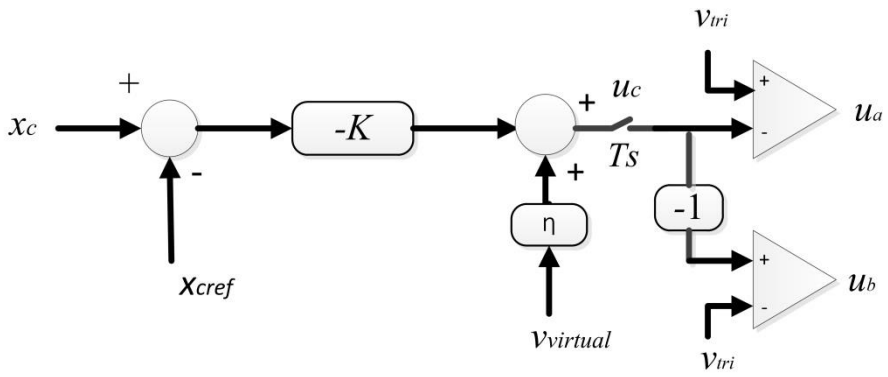

Figure 5.2: Voltage control implemented for generating (non)sinusoidal voltages.

The experimental setup is shown in Figure 5.3. It consists of a computer connected to a dSPACE DS1103 via optical fiber for real time interfacing. The PWM signals generated by the dSPACE DS1103 is given to the power inverter. The power inverter is an IGBT Inverter module of 2 kW, model 8857-1 of Labvolt. The inverter is also excited with a DC power supply that provides maximum of 200 Vdc. A 2 mH inductor and 5 µF capacitors are connected to the output of the inverter for control and filtering. The filtered voltage is then given to the primary side of a 200 VA 25V/24V transformer and a resistive load of 2.8 ohms connected to its secondary. Appropriate current and voltage probes based on Hall effect were connected at the

low and high voltage sides of test transformer to capture the voltages and currents signals. The waveforms were digitized using ADC (analog to digital channel) of dSPACE DS1103 and recorded in the PC using the software control desk. The data were then processed in MATLAB for analysis and losses computation. The losses were calculated by subtracting power at primary from the power at the secondary of the transformer. IEEE standards [61] were followed while conduction the tests.

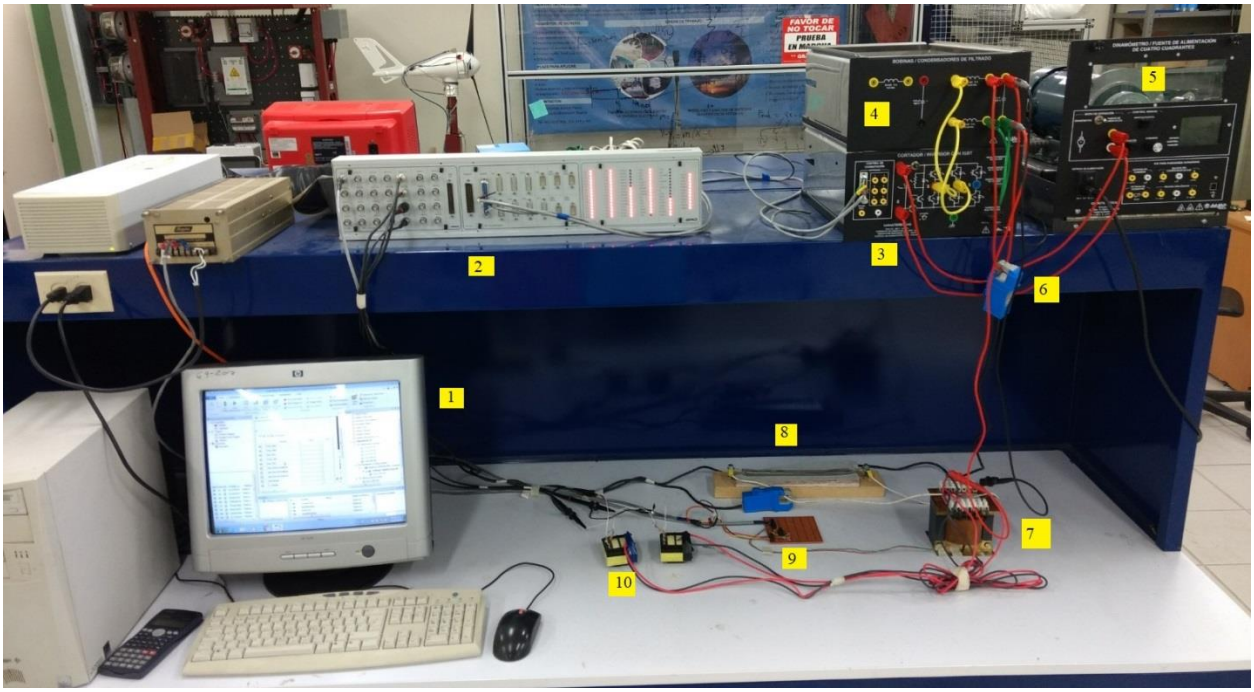

Figure 5.3: Experimental setup; 1) PC 2) dSPACE 3) Inverter 4) filter 5) DC voltage source 0 to 200 V 6) current sensor 7) 200 VA transformer 8) Resistive load 9) Temperature sensor 10) Voltage sensors.

Fundamental parameters of the test transformer are summarized in Table 5.1. The sinusoidal and non-sinusoidal voltage signals were generated with a sampling rate of 5 kHz. The highest harmonic and interhamonic frequency that can be superimposed on fundamental implemented using MATLAB/Simulink in this work is equal to 1/10th of the sampling rate. In the control

system applied, a proper control with the block of dSPACE inverter is required in MATLAB/Simulink which provides the PWM signals to the inverter. PWM changes with the applied reference to generate the desired waveform at the output of the inverter. Hence, for 5 kHz rate, 9th ($=\frac{1}{10^{\text{th}}}.5$ kHz) [60] is the maximum harmonic that is generated. The MATLAB/Simulink implementation is shown in Figure 5.4.

Table 5.1: Tested transformer parameters.

Specifications	Value
Apparent power	200 VA
Frequency	60 Hz
High voltage side (primary)	125 Vrms
Low voltage side	24 Vrms
Primary current	1.6 A
Secondary current	8.33 A

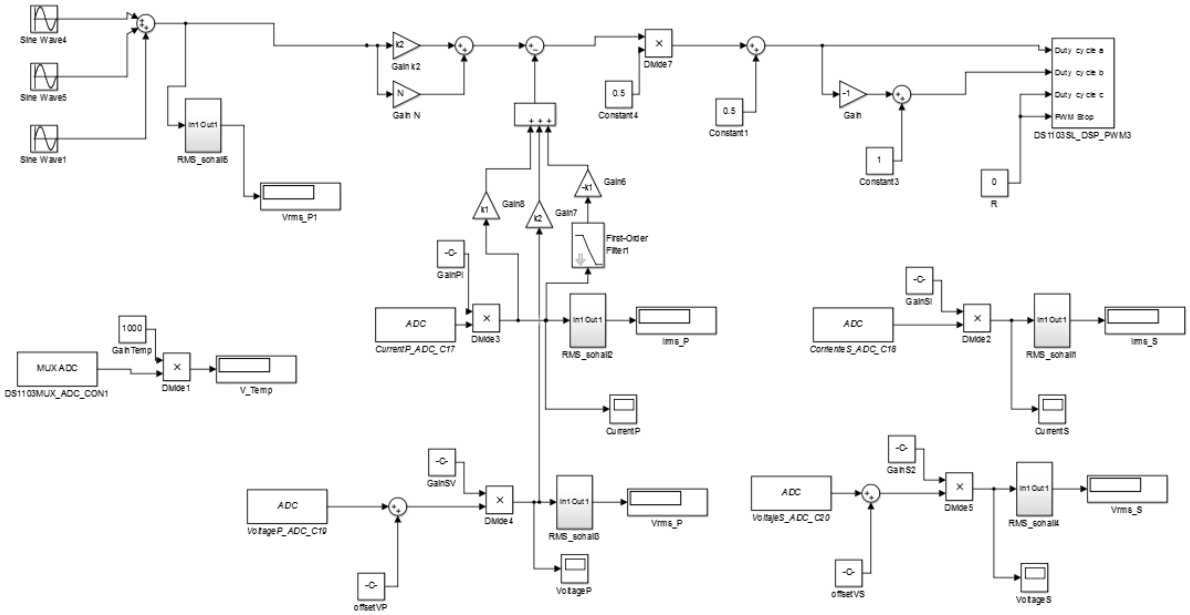

Figure 5.4: Closed loop control arrangement in MATLAB/Simulink.

The dSPACE DS1103 platform allows the connection between the simulation model and the hardware, since it has input and output modules for analog and digital signals, which together with the ControlDesk software allows to have the closed loop between the elements involved in the study.

The single-phase inverter is a controlled pulse width modulation (PWM), with a switching frequency of 5 kHz and is powered by a DC voltage source. The application of the control signal for the inverter involves the PWM ports of the dSPACE DS1103 platform.

To monitor the temperature of the transformer winding, an RTD PT 100 sensor was connected to dSPACE via Wheatstone bridge for amplification using TL084 IC. It was then connected to dSPACE via Wheatstone bridge. It helps in amplifying voltage using TL084 IC. The Wheatstone bridge has the characteristic of providing very small differential voltages between points "a" and "b" (output) shown in Figure 5.5 depending on the change of value of the sensor resistor with temperature.

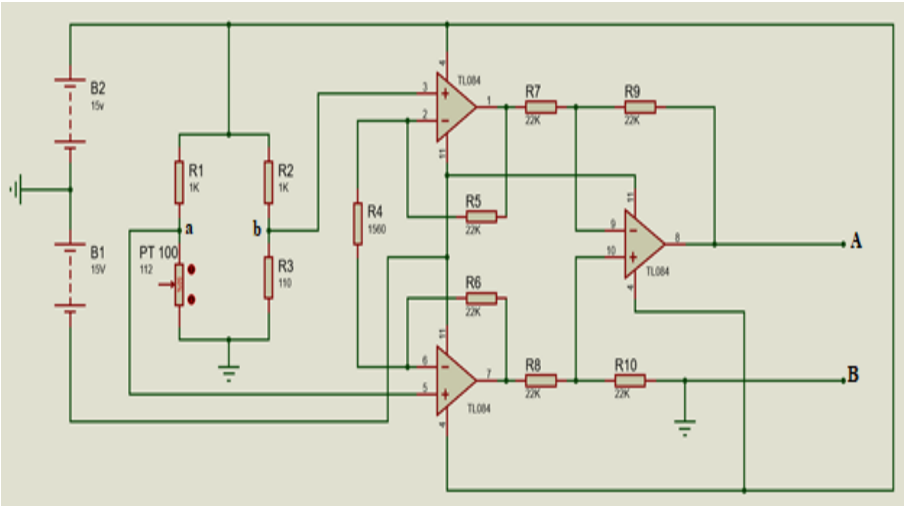

Figure 5.5: Wheatstone bridge and TL084 amplifier.

For example, if R1 = R2 = 1 kΩ and PT100 = R3 = 110 Ω, it could be said that the bridge is in equilibrium (0V between points a and b) by the cross-multiplication rule (R1 * R3 = R2 * PT100). Therefore, a slight variation in the value of the resistors causes a very small change in the output voltage of the bridge, which is then amplified at the output with the use of an amplifier.

After designing the circuit, it was assembled on a test board and its operation was tested. The implementation was done on a phenolic plate for immediate use as shown in figure 5.6.

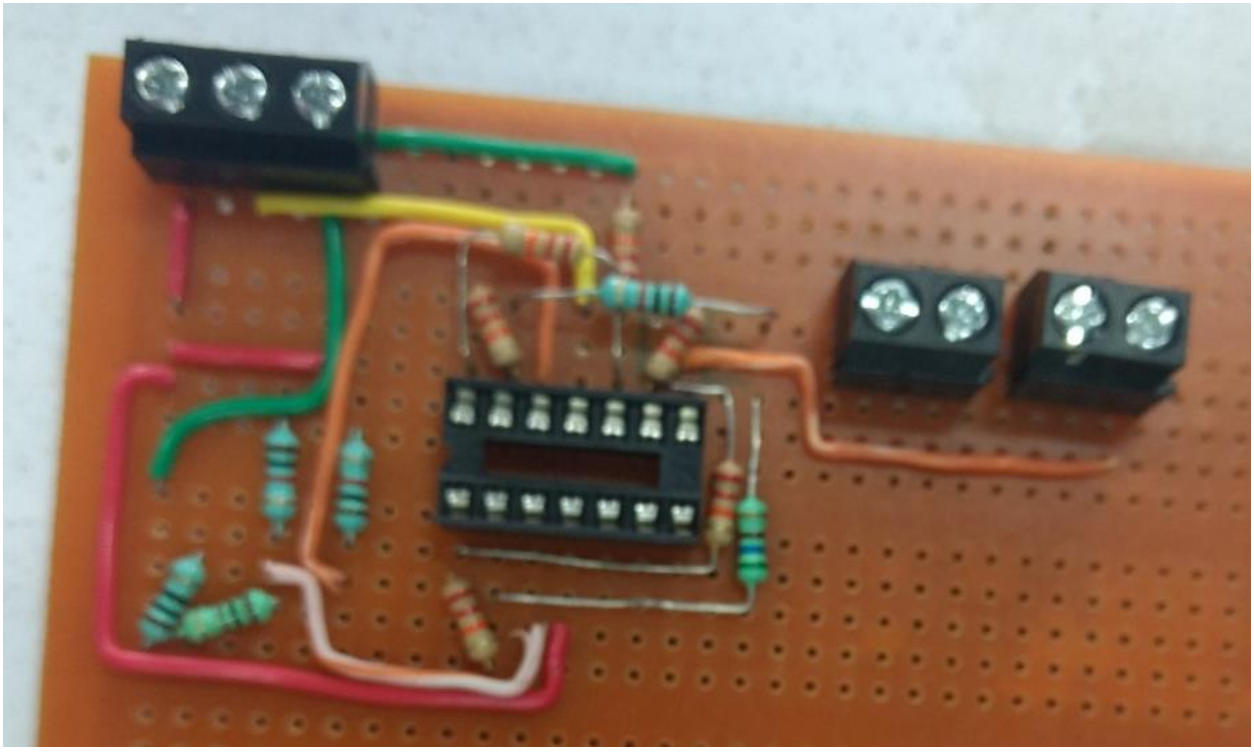

Figure 5.6: Implemented Wheatstone bridge and ICs.

The RTD PT 100 sensor was calibrated with the help of a multimeter having thermometer function based on a thermocouple type K. The output voltage signal of the circuit was recorded while increasing the temperature of the oil having RTD and multimeter dipped. The multimeter

sensor and the RTD PT 100 were immersed in oil at room temperature and the temperature of the oil was increased using soldering iron (see Figure 5.7).

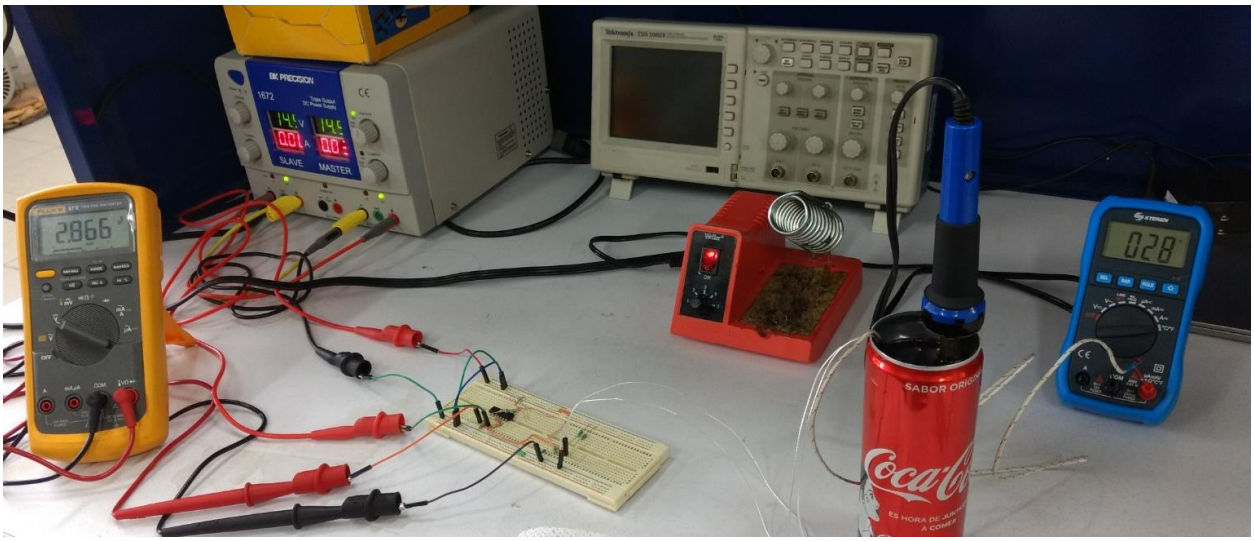

Figure 5.7: Sensor calibration.

The temperature and voltages were recorded, for example: 34 ° C had a voltage of 2.92 V. The temperature varied from 28 ° C to 82 ° C and the voltage from 1.88 V to 9.38 V.

5.2 MODELLING FOR LOSSES COMPUTATION

A non-sinusoidal current or voltage in a steady state condition has fundamental and harmonic components. Fourier series of the alternating voltage or current signal is as follows:

$$v(t) = V_{dc} + \sum_{n=0}^{n_{max}} \sqrt{2}\, V_n \sin(h\omega_0 t + \alpha_n) \tag{5.9}$$

$$i(t) = I_{dc} + \sum_{n=1}^{n_{max}} \sqrt{2}\, I_n \sin(h\omega_0 t + \beta_n) \tag{5.10}$$

where

V_{dc} : dc component of $v(t)$.

I_{dc} : dc component of I_{dc} .

n_{max} : Maximum harmonic or interharmonic order in the signal.

V_n : rms voltage of harmonic order *n.*

I_n :rms current of harmonic order *n*.

ω_0 : Fundamental angular speed.

α_n : Phase angle of harmonic or interharmonic voltage.

β_n : Phase angle of harmonic or interharmonic current.

The active power in non-sinusoidal condition is given as follows,

$$P = V_{dc} I_{dc} + \sum_{n=1}^{n_{max}} V_n\, I_n \cos(\theta_n) \tag{5.11}$$

The losses were calculated by subtracting power at the secondary minus power at the primary of transformer.

5.3 RESULTS AND ANALYSIS

The tests were conducted in a temperature-controlled environment for maintaining the ambient temperature throughout the experiment.

The aim of the tests was to observe the increase in losses and temperature due to harmonics injection with different amplitudes. Different harmonics and interharmonics up to 11th order (660 Hz) were excited on the primary side of the transformer with low voltage side connected to the nominal load. Each harmonic frequency with zero angles was superimposed on fundamental at different instant of time. The data were recorded and Short Time Fourier Transform (STFT) was applied to compute losses in the transformer.

Figure 5.7 shows the injection of 10 % of 3rd harmonic in the fundamental frequency voltage. From the Figure, it can be observed that the voltage gets distorted after 300 seconds. In Figure 5.8, 20 % of the 3rd harmonic is added to the fundamental for testing transformer.

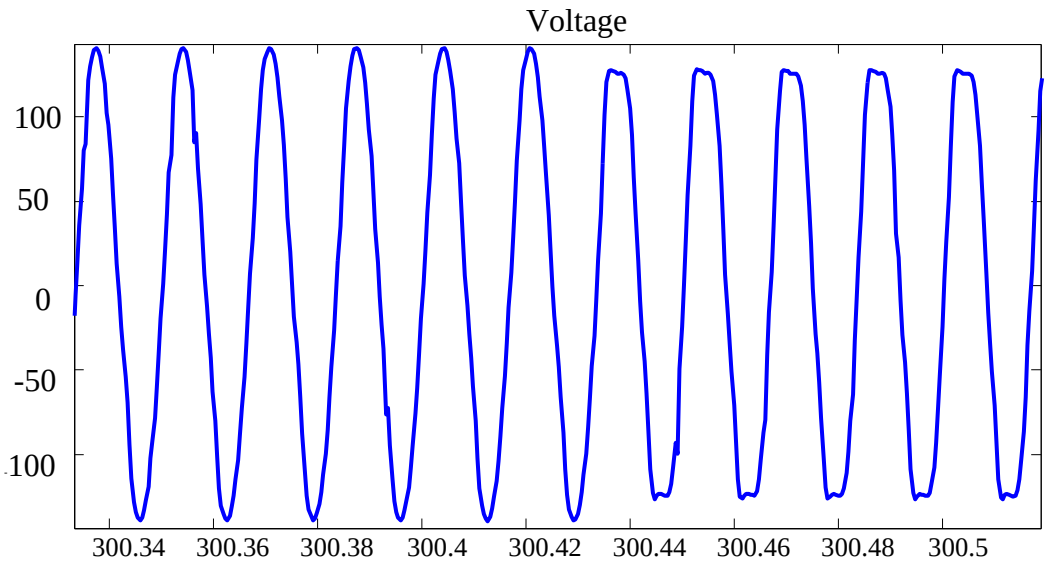

Figure 5.8: Injection of 10 % of 3rd harmonic into fundamental.

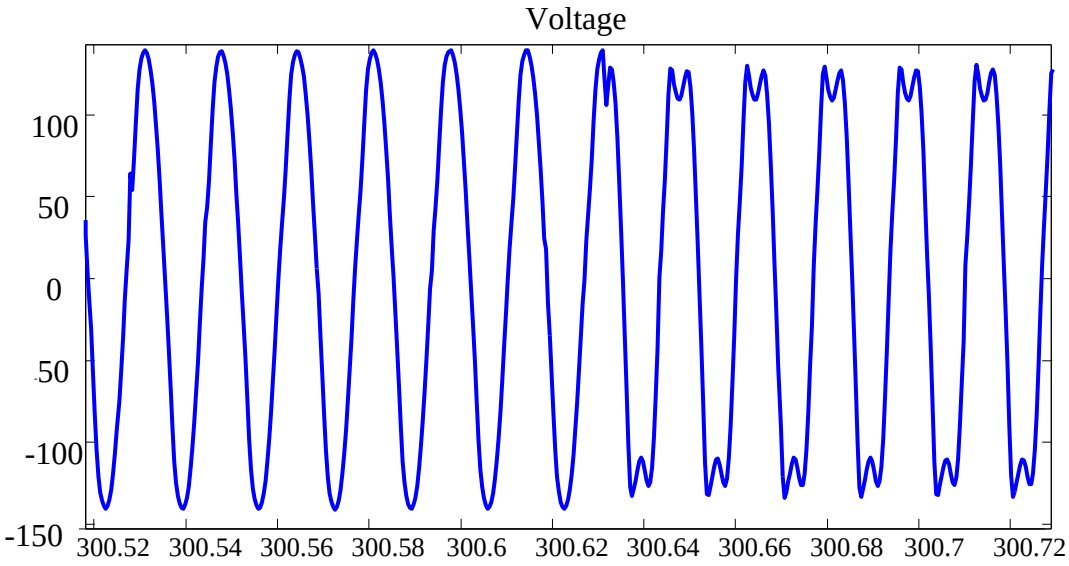

Figure 5.9: Injection of 20 % of 3rd harmonic into fundamental.

The losses due to different harmonics with different amplitudes are shown in Figure 5.9. These results are good in agreement with the measured results obtained in [62] and [63].

Figure 5.10: Transformer losses due to different harmonics.

Table 5.2 demonstrates the temperature increase in transformer windings due to harmonics. The temperature was monitored for 2 and the half hours as it was the time the temperature windings took to reach its maximum. It can be observed that increasing the 3rd harmonic amplitude, the temperature increases.

Table 5.2: Temperature increase in transformer windings due to harmonics.

Harmonic	Time taken	Temperature in °C
Fundamental	2 hours	56.85 °C
Fundamental + 5% of 3^{rd} Harmonic	2 hours 30 minutes	60.11 °C
Fundamental + 10% of 3^{rd} Harmonic	2 hours 30 minutes	61.09 °C
Fundamental + 15% of 3^{rd} Harmonic	2 hours 30 minutes	61.56 °C
Fundamental + 20% of 3^{rd} Harmonic	2 hours 30 minutes	62.20 °C

The next objective of the experimental setup was to generate interharmonics and pass them through the transformer for losses evaluation. Unfortunately, due to COVID-19 pandemic, the laboratory got closed and the work could not be preceded further. Other important development planned was to inject harmonics and interharmonics with 90 degree and 180 degree angles into transformer. The effects of harmonics and interharmonics with angles have never been studied in the literature. With the applied control, it was possible to conduct such study.

Since there is infinite number of combination of interharmonics, making it difficult to decide which of them must be considered for testing in the laboratory, it is preferable that a realistic scenario based on simulation-based study must be done to obtain harmonic and interharmoic spectrum and study the transformer losses. For this purpose, a cycloconverter coupled with a rectifier in parallel has been simulated and the spectrum has been obtained (shown in figure 5.10

and 5.11). The idea is to generate this distorted voltage signal and apply it across the transformer and develop a complete analysis under harmonic and interharmonic condition.

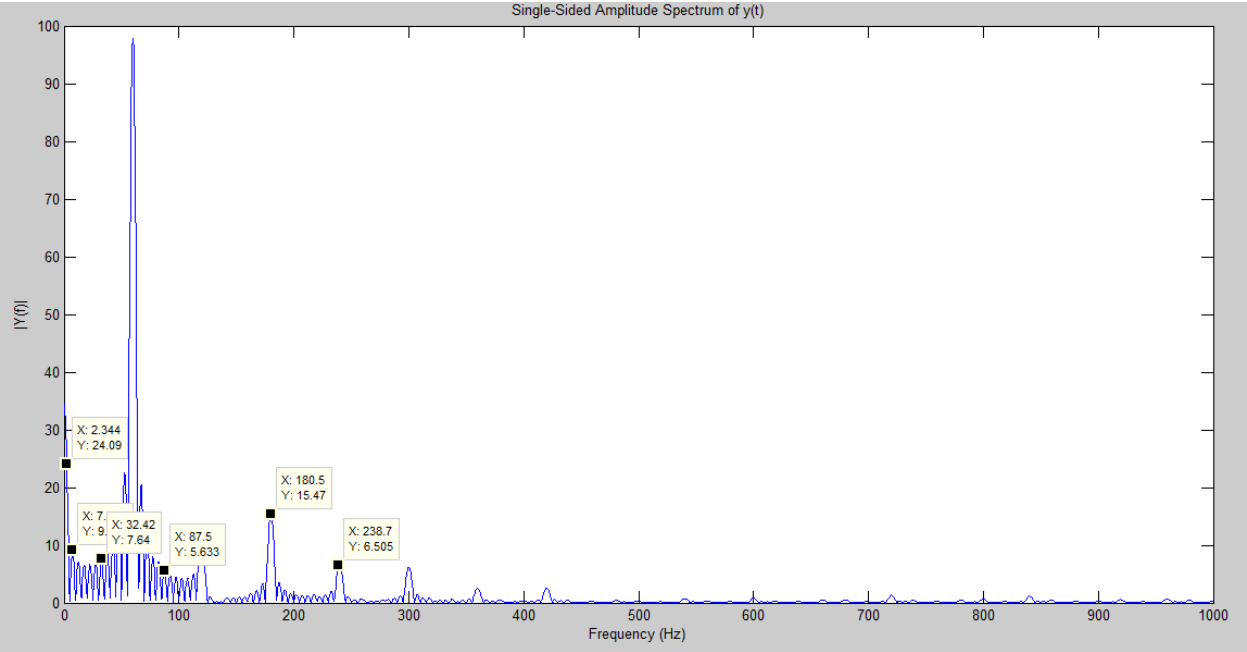

Figure 5.11: Cycloconverter spectrum with output frequency 30 Hz.

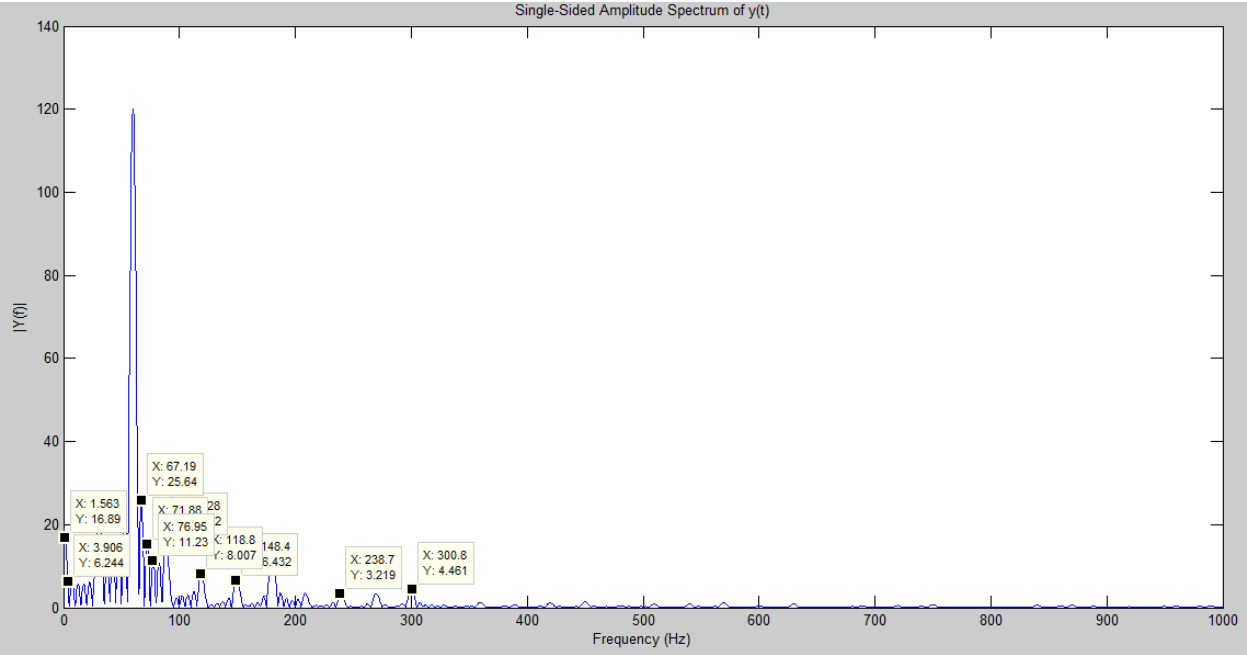

Figure 5.12: Cycloconverter with output frequency 15 Hz.

To complete the experimental work, the following are the steps to follow:

1. Following the IEEE standards [5], combination of harmonic voltages need to be generated for transformer impacts evaluation.
2. Following the IEEE standards [5], Interharmonic voltages need to be generated for transformer impacts evaluation.
3. Harmonic and Interharmonic spectrum can be obtained from the distribution system or industry and generate the voltages containing both, for transformer impacts evaluation.
4. Impacts of harmonic and interharmonic components of the loads such as shown in Figure 5.10 (a) and 5.10 (b) need to be applied across the transformer for impacts evaluation.
5. Impacts of different harmonics and interharmonics angles can be evaluated using the established experimental setup in this chapter.

Chapter 6. CONCLUSIONS AND FUTURE WORKS

In this chapter, conclusions, and future works are given.

6.1 CONCLUSIONS

The impact of distortion in voltage and current on transformers, and the solutions proposed in pertinent literature are summarized in Figure 6.1. By carrying out an exhaustive survey of the situation, the problem and solutions can be better understood and aspects of the study can be reflected and applied in future work. From the research work discussed in this survey, it is seen that the harmonic and interharmonic distortions cause: additional power losses, temperature rise, accelerated aging, and core saturation in distribution transformers.

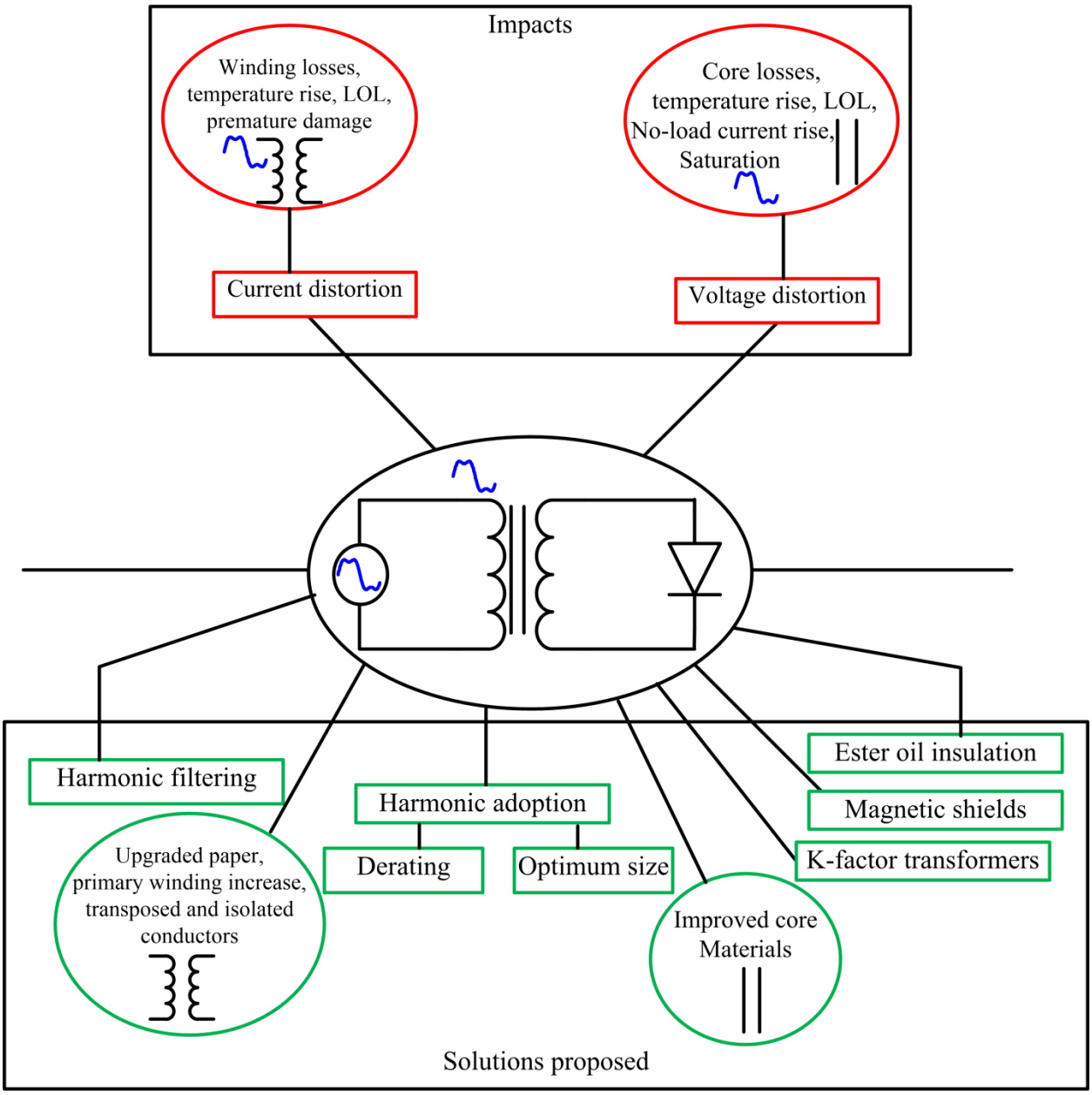

Figure 6.1: General outlook of the transformer problems caused by the distortion in voltage and currents, and the proposed solutions.

The impact of voltage harmonics and angles on no-load losses, together with an unbalanced supply voltage, has been studied in-depth, whereas the effect of interharmonics and their angles are needed to be analyzed further. Moreover, work evaluating the impacts of the simultaneous occurrence of unbalanced, harmonic, and interharmonic voltage on transformer cores needs to be

carried out. The harmonic and interharmonic angles must also be included in this research to ensure a comprehensive study. The impacts of distortions in voltage and current on transformer vibration must also be evaluated.

To reduce the effects of current and voltage distortions on windings, upgraded paper, increase of primary windings, transposed and isolated conductors, and electrostatic shields are the methods that can be considered by the industry to increase the efficiency and reliability of the transformers. To reduce the undesirable effects in the core, improved core materials and laminated cores are the strategies that can be employed in the industry. Other solutions are K -factor transformers, filtering, oversizing, and derating. In general, filtering and derating are the two commonly used techniques to decrease the effects of non-linear loading and therefore, to ensure transformer reliability. The derating is one of the low-cost approaches, while filtering is another effective way to dispose of harmonic problems.

New analytical formulas for the EMF and EC loss computation in transformer tank covers have been strictly derived, with proper consideration of harmonics in the load current. Noteworthy, asymptotic formulas were formally obtained using asymptotic approximations of the modified Bessel functions that allowed to simplify further the expressions making them easier to implement in engineering software. These formulas allow the distribution of MF and computation of power losses due to each harmonic in the tank wall. The geometry considered accurately represents the arrangement of the conductor carrying load current with harmonics passing through the transformer tank wall.

The new formulas for calculating EMF and EC losses in transformer tank wall were successfully verified by comparing their performance with computationally expensive FEM simulations, proving their efficiency and efficacy. Hence, our results are useful for industrial

applications, where transformer analysis and design demand accurate results and low-cost computational resources. It has been additionally shown that the presence of harmonics in the load current lowers the skin effect depth, they considerably increase stray losses and therefore must be taken into account for proper analysis and design of transformers. These formulas can be employed in the design algorithms for evaluating the impacts of harmonics on the transformer tank wall. The results can be used to improve the design of transformer and thereby considerably reduce the possibility of hot spots in the bushing regions. Therefore, our formulas are an important advancement to the existing methods and formulas available in the literature.

6.2 FUTURE WORKS

The impact of voltage harmonics and angles on no-load losses, together with an unbalanced supply voltage, has been studied in-depth, whereas the effect of interharmonics and their angles are needed to be analyzed further. Moreover, work evaluating the impacts of the simultaneous occurrence of unbalanced, harmonic, and interharmonic voltage on transformer cores needs to be carried out. The harmonic and interharmonic angles must also be included in this research to ensure a comprehensive study. The impacts of distortions in voltage and current on transformer vibration must also be evaluated.

The significant increase of plug-in EVs and integration of renewable energy systems in the distribution network can overload the distribution transformers. The effect of the above on overload and unbalanced supply of distorted currents and voltages must be investigated, also, that of supraharmonics (frequencies above 2 kHz), on distribution transformer is worth investigation. In the presence of harmonic and interharmonic distortion, resonance might occur

between the transformer impedance and system capacitance which may lead to stresses on windings. Such studies could be of interest regarding the useful life of a transformer.

Despite the recent developments carried out in transformer research under non-linear loading, there are still several issues that require further attention of the researchers. Several design approaches can be simultaneously studied in non-linear conditions and comparisons made to arrive at the best possible solution. The impacts of harmonics, interharmonics and their angles, unbalanced currents and voltages, and DC offset cannot be ignored and needs to be considered before designing a transformer.

The possible solutions that could be considered by the industry to reduce the effects of non-linear loads are: increase primary windings, improve core materials, magnetic shunts, improve the tank wall geometry, a filter at the point of common coupling, connections for mitigating harmonics, and use of transposed and isolated conductors. Studies on each method above need to be carried out either individually or combining more than one, to develop mathematical models for transformer design improvement. Magnetic shunts in the tank wall and other parts have been proved to be highly useful in reducing losses in transformers. But no study has been presented in fact to investigate their effectiveness in improving transformer efficiency under non-sinusoidal operation. Their integration in the tank walls is not costly as the leftover material from core construction and other parts can be reused. For calculating optimum packets, the relation between magnetic flux density and lamination packets need to be developed. The losses in the tank wall due to harmonics increase considerably because they decrease skin-depth, resulting in the magnetic flux density increase.

In the presence of distortions, magnetic yoke shields can be employed to return a large portion of the axial leakage flux to the transformer. Also, purely non-metallic material for core clamping

with magnetic shields can be used to reduce the harmonic effects. The stray flux can be controlled by magnetic shunts of core laminations installed inside the tank wall. Regarding transformer connections, the effects of different transformer connections and vector groups on interharmonic cancellation have not been studied.

In the transformer sizing problem, considering unbalanced, harmonic and interharmonic voltages with angles would be another important development.

If the load is such that derating is required, a mixed and combined approach based on TSFEM provides the most accurate study of the transformer, because it can consider all the geometrical specifications, material properties, unbalances, distortion in voltage and current, and a no-load operation. Along with the harmonic spectrum, the information and details regarding their angles, unbalanced voltage harmonics and interharmonics, and also DC offset must be given to industry to derate a transformer. Furthermore, the hot-spot temperature is the most prominent factor in estimating the transformer LOL, and therefore, it can be a reliable parameter for derating or validating such methods. Besides, derating methods based on temperature rise and LOL sound more rational than that based on losses calculations. This will allow taking into account the insulation properties of the material that influence transformer life span. The force applied by the electromagnetic field on the windings and core has not been studied under non-sinusoidal operation. The effect of core temperature on the winding must be investigated and should it influence the winding hot-spots, an appropriate method to include it in the derating process must be developed.

Moreover, the analytical approach for calculating stray losses in transformer tank wall provides basis for further developments such as analysis of stray losses in the case of three-phase currents (three conductors passing through the tank wall). This approach can also be extended to

calculate losses in windings and core, providing a powerful tool for transformer derating, and thus improve the reliability and efficiency of the transformer.

REFERENCES

[1] J. Faiz and M. Soleimani, "Dissolved Gas Analysis Evaluation using Conventional Methods for Fault Diagnosis in Electric Power Transformers- A Review," *IEEE Trans. Dielectr. Electr. Insul.*, vol. 24, pp. 1239–1248, Apr. 2017.

[2] M. Ghazizadeh, J. Faiz, and H. Oraee, "Derating of distribution transformers under non-linear loads using a combined analytical-finite elements approach," *IET Electr. Power Appl.*, vol. 10, no. 8, pp. 779–787, 2016.

[3] M. Yazdani-Asrami, M. Mirzaie, and A. A. Shayegani Akmal, "No-load loss calculation of distribution transformers supplied by nonsinusoidal voltage using three-dimensional finite element analysis," *Energy*, vol. 50, pp. 205–219, 2013.

[4] A. Kalair, N. Abas, A. R. Kalair, Z. Saleem, and N. Khan, "Review of harmonic analysis, modeling and mitigation techniques," *Renew. Sustain. Energy Rev.*, vol. 78, pp. 1152–1187, 2017.

[5] "IEEE Recommended Practice and Requirements for Harmonic Control in Electric Power Systems," *IEEE Std 519-2014 (Revision of IEEE Std 519-1992)*. pp. 1–29, 2014.

[6] J. Lu, X. Zhao, and S. Yamada, "Introduction to Harmonic Balance Finite Element Method (HBFEM)," in *Harmonic Balance Finite Element Method: Applications in Nonlinear Electromagnetics and Power Systems*, IEEE, 2016, pp. 1–18.

[7] J. Faiz, M. Ghazizadeh, and H. Oraee, "Derating of transformers under non-linear load current and non-sinusoidal voltage – an overview," *IET Electr. Power Appl.*, vol. 9, no. 7, pp. 486–495, 2015.

[8] J. Faiz, B. M. Ebrahimi, and M. Ghofrani, "Mixed Derating of Distribution Transformers Under Unbalanced Supply Voltage and Nonlinear Load Conditions Using TSFEM," *IEEE Trans. Power Deliv.*, vol. 25, no. 2, pp. 780–789, 2010.

[9] C. AJ, M. A. Salam, Q. M. Rahman, F. Wen, S. P. Ang, and W. Voon, "Causes of transformer failures and diagnostic methods – A review," *Renew. Sustain. Energy Rev.*, vol. 82, pp. 1442–1456, 2018.

[10] S. Khan, R. Escarela-Perez, J. C. Olivares-Galvan, V. M. Jimenez-Mondragon, and F. P. Espino-Cortés, "Finite element analysis of distribution transformer under harmonics condition: A review," in *2017 IEEE International Autumn Meeting on Power, Electronics*

and Computing (ROPEC), 2017, pp. 1–5.

[11] A. Khallawi, H. Zainuddin, F. Hanaffi, and R. Chyad, "Transformer Oil Diagnostic by Using an Optical Fibre System: A Review," *IET Sci. Meas. ? Technol.*, Mar. 2019.

[12] S. Maximov, J. C. Olivares, S. Magdaleno-Adame, R. Escarela-Perez, and E. Campero-Littlewood, "New Analytical Formulas for Electromagnetic Field and Eddy Current Losses in Bushing Regions of Transformers," *IEEE Trans. Magn.*, vol. 51, pp. 1–10, Apr. 2015.

[13] P. Penabad-Duran, X. M. Lopez-Fernandez, and J. Turowski, "3D non-linear magneto-thermal behavior on transformer covers," *Electr. Power Syst. Res.*, vol. 121, Apr. 2015.

[14] S. L. Ho, Y. Li, R. Y. Tang, K. W. E. Cheng, and Y. Shiyou, "Calculation of Eddy Current Field in the Ascending Flange for the Bushings and Tank Wall of a Large Power Transformer," *Magn. IEEE Trans.*, vol. 44, pp. 1522–1525, Jul. 2008.

[15] A. Turowski, J.; Pelikant, "Eddy current losses and hot-spot evaluation in cover plates of power transformers," *IEE Proc.-Electr. Power Appl.*, vol. 144, no. 6, p. 435–440., 1997.

[16] D. M. Del Vecchio, R. M.; Poulin, B.; Feeney, M. E. F.; Feghali, P. T.; Shah, D. M.; Ahuja, R.; Shah, *Transformer design principles: with applications to core-form power transformers*. CRC press, 2001.

[17] G. W. Massey, "Estimation methods for power system harmonic effects on power distribution transformers," *IEEE Trans. Ind. Appl.*, vol. 30, no. 2, pp. 485–489, 1994.

[18] E. F. Fuchs and M. A. S. B. T.-P. Q. in P. S. and E. M. Masoum, Eds., "Chapter 2 - Harmonic Models of Transformers," Burlington: Academic Press, 2008, pp. 55–108.

[19] Y. Liu, G. T. Heydt, and R. F. Chu, "The power quality impact of cycloconverter control strategies," *IEEE Trans. Power Deliv.*, vol. 20, no. 2, pp. 1711–1718, 2005.

[20] E. F. Fuchs and M. A. S. B. T.-P. Q. in P. S. and E. M. Masoum, Eds., "Chapter 1 - Introduction to Power Quality," Burlington: Academic Press, 2008, pp. 1–54.

[21] "IEEE Draft Recommended Practice for Establishing Liquid-Immersed and Dry-Type Power and Distribution Transformer Capability When Supplying Nonsinusoidal Load Currents," *IEEE PC57.110/D6.1, February 2018*. pp. 1–72, 2018.

[22] A. Elmoudi, M. Lehtonen, and H. Nordman, "Corrected winding eddy-current harmonic loss factor for transformers subject to nonsinusoidal load currents," in *2005 IEEE Russia Power Tech*, 2005, pp. 1–6.

[23] T. D. Kefalas and A. G. Kladas, “Harmonic Impact on Distribution Transformer No-Load Loss,” *IEEE Trans. Ind. Electron.*, vol. 57, no. 1, pp. 193–200, 2010.

[24] M. Digalovski, K. Najdenkoski, and G. Rafajlovski, “Impact of current high order harmonic to core losses of three-phase distribution transformer,” in *Eurocon 2013*, 2013, pp. 1531–1535.

[25] S. V. Kulkarni and S. A. Khaparde, “Transformer Engineering Design, Technology, and Diagnostics,” *CRC Press*, vol. 2, 2012.

[26] A. Testa *et al.*, “Interharmonics: Theory and Modeling,” *IEEE Trans. Power Deliv.*, vol. 22, no. 4, pp. 2335–2348, 2007.

[27] D. Gallo, R. Langella, A. Testa, and A. Emanuel, “On the effects of voltage subharmonics on power transformers: a preliminary study,” in *2004 11th International Conference on Harmonics and Quality of Power (IEEE Cat. No.04EX951)*, 2004, pp. 501–506.

[28] R. Langella, A. Testa, and A. E. Emanuel, “On the Effects of Subsynchronous Interharmonic Voltages on Power Transformers: Single Phase Units,” *IEEE Trans. Power Deliv.*, vol. 23, no. 4, pp. 2480–2487, 2008.

[29] R. Langella, A. Testa, and A. E. Emanuel, “On the Effects of Subsynchronous Interharmonic Voltages on Power Transformers: Three Phase Units,” *IEEE Trans. Power Deliv.*, vol. 23, no. 4, pp. 2461–2471, 2008.

[30] E. Arslan, S. Sakar, and M. E. Balci, “On the no-load loss of power transformers under voltages with sub-harmonics,” in *2014 IEEE International Energy Conference (ENERGYCON)*, 2014, pp. 228–233.

[31] S. Taheri, A. Gholami, I. Fofana, and H. Taheri, “Modeling and simulation of transformer loading capability and hot spot temperature under harmonic conditions,” *Electr. Power Syst. Res.*, vol. 86, pp. 68–75, 2012.

[32] I. Iskender and A. Najafi, “Evaluation of transformer performance under harmonic load based on 3-D time stepping finite element method,” in *2014 16th International Conference on Harmonics and Quality of Power (ICHQP)*, 2014, pp. 224–228.

[33] A. Baggini and Z. Hanzelka, “Voltage and Current Harmonics,” *Handbook of Power Quality*. pp. 187–261, 18-Apr-2008.

[34] P. N. Korovesis, G. A. Vokas, I. F. Gonos, and F. V Topalis, “Influence of large-scale installation of energy saving lamps on the line Voltage distortion of a weak network

supplied by photovoltaic station," *IEEE Trans. Power Deliv.*, vol. 19, no. 4, pp. 1787–1793, 2004.

[35] P. S. Moses, M. A. S. Masoum, and K. M. Smedley, "Harmonic losses and stresses of nonlinear three-phase distribution transformers serving Plug-In Electric Vehicle charging stations," in *ISGT 2011*, 2011, pp. 1–6.

[36] M. A. Awadallah, B. Venkatesh, and B. N. Singh, "Impact of Solar Panels on Power Quality of Distribution Networks and Transformers," *Can. J. Electr. Comput. Eng.*, vol. 38, no. 1, pp. 45–51, 2015.

[37] M. A. Awadallah, T. Xu, B. Venkatesh, and B. N. Singh, "On the Effects of Solar Panels on Distribution Transformers," *IEEE Trans. Power Deliv.*, vol. 31, no. 3, pp. 1176–1185, 2016.

[38] M. Bagheri, A. Subramaniam, S. Bhandari, S. Chandar, and S. K. Panda, "Residential lighting influence on cast-resin distribution transformer aging rate," in *2015 IEEE International Conference on Building Efficiency and Sustainable Technologies*, 2015, pp. 45–49.

[39] P. S. Moses and M. A. S. Masoum, "Three-Phase Asymmetric Transformer Aging Considering Voltage-Current Harmonic Interactions, Unbalanced Nonlinear Loading, Magnetic Couplings, and Hysteresis," *IEEE Trans. Energy Convers.*, vol. 27, no. 2, pp. 318–327, 2012.

[40] L. W. Pierce, "Transformer design and application considerations for nonsinusoidal load currents," *IEEE Trans. Ind. Appl.*, vol. 32, no. 3, pp. 633–645, 1996.

[41] J. Zheng, "TRANSFORMER AC WINDING RESISTANCE AND DERATING WHEN SUPPLYING HARMONIC-RICH CURRENT," Michigan Technological University, 2000.

[42] S. L. Ho, Y. Li, H. C. Wong, S. H. Wang, and R. Y. Tang, "Numerical simulation of transient force and eddy current loss in a 720-MVA power transformer," *IEEE Trans. Magn.*, vol. 40, no. 2, pp. 687–690, 2004.

[43] C. Guerin, G. Tanneau, and G. Meunier, "3D eddy current losses calculation in transformer tanks using the finite element method," *IEEE Trans. Magn.*, vol. 29, no. 2, pp. 1419–1422, 1993.

[44] R. D. Henderson and P. J. Rose, "Harmonics: the effects on power quality and

transformers," *IEEE Trans. Ind. Appl.*, vol. 30, no. 3, pp. 528–532, 1994.

[45] B. P. Das and Z. Radakovic, "Is Transformer kVA Derating Always Required Under Harmonics? A Manufacturer's Perspective," *IEEE Trans. Power Deliv.*, vol. 33, no. 6, pp. 2693–2699, 2018.

[46] R. Lucas, N.R.Jayasinghe, and K. Perera, "Power system harmonic effects on distribution transformers and new design consideration for k factor transformers," Aug. 2005.

[47] J. G. Boudrias, "Harmonic mitigation, power factor correction and energy saving with proper transformer and phase shifting techniques," in *Canadian Conference on Electrical and Computer Engineering 2004 (IEEE Cat. No.04CH37513)*, 2004, vol. 1, p. 133–136 Vol.1.

[48] S. A. Deokar and L. M. Waghmare, "Impact of power system harmonics on insulation failure of distribution transformer and its remedial measures," in *2011 3rd International Conference on Electronics Computer Technology*, 2011, vol. 3, pp. 136–140.

[49] E. Hajipour, M. Mohiti, N. Farzin, and M. Vakilian, "Optimal distribution transformer sizing in a harmonic involved load environment via dynamic programming technique," *Energy*, vol. 120, pp. 92–105, 2017.

[50] A. Njafi and I. Iskender, "A novel concept for derating of transformer under unbalance voltage in the presence of non linear load by 3-D finite element method," *Electr. Eng.*, vol. 97, Mar. 2015.

[51] V. S. Vladimirov, *Equations of mathematical physics*. Moscow, 1984.

[52] F. W. Olver, *Asymptotics and Special Functions*. New York and London: Academic Press, 1974.

[53] C. W. Olver, F. W.; Lozier, D. M.; Boisvert, R. F.; Clark, *NIST Handbook of mathematical functions*. Cambridge University Press, 2010.

[54] W. H. Hayt, *Engineering electromagnetics,*. Singapore,: McGraw-Hill Book Company, 1989.

[55] A. Pramanik, *Electromagnetism: theory and applications,*. New Delhi: Prentice Hall of India Private Limited, 2008.

[56] N. Ida, *Numerical modeling for electromagnetic non-destructive evaluation*. London: Chapman & Hall, 1995.

[57] C J Carpenter., "Comparison of alternative formulations of 3-dimensional magnetic-field

and eddy-current problems at power frequencies.," *IEE Proc.*, 1977.

[58] O. Biro, "Edge element formulations of eddy current problems.," *Comput. Methods Appl. Mech. Eng.*, vol. 169, pp. 391–405, 1999.

[59] M. Dargahi Kafshgarkolaei, "Stability analysis and implementation of Power-Hardware-in-the-Loop for power system testing.," Queensland University of Technology, 2015.

[60] Z. Ali, N. Christofides, L. Hadjidemetriou, and E. Kyriakides, "Diversifying the Role of Distributed Generation Grid-Side Converters for Improving the Power Quality of Distribution Networks Using Advanced Control Techniques," *IEEE Trans. Ind. Appl.*, vol. 55, no. 4, pp. 4110–4123, 2019.

[61] "C57.123-2019 - IEEE Guide for Transformer Loss Measurement."

[62] E. F. Fuchs and R. Fei, "A new computer-aided method for the efficiency measurement of low-loss transformers and inductors under nonsinusoidal operation," *IEEE Trans. Power Deliv.*, vol. 11, no. 1, pp. 292–304, 1996.

[63] T. Stensland, E. F. Fuchs, W. M. Grady, and M. T. Doyle, "Modeling of magnetizing and core-loss currents in single-phase transformers with voltage harmonics for use in power flow," *IEEE Trans. Power Deliv.*, vol. 12, no. 2, pp. 768–774, 1997.